Electronic Supplementary Material (ESI)

for

Evaluation of Structurally Related Acyclic Ligands OBETA, EHDTA, and EGTA for Stable Mn^{2+} Complex Formation

Elena Grattoni,[a] Fabio Travagin,[b] Ferenc Kálmán,[c] Zsolt Baranyai,[d] Roberto Negri,[b,e] Fabio Carniato,[f] Giovanni B. Giovenzana,[b] Carlos Platas-Iglesias,[g] Mauro Botta*[f]

[a] Dip. di Scienze Chimiche e Farmaceutiche, Università di Trieste, Piazzale Europa 1, 34127 Trieste (TS), Italy

[b] Dip. di Scienze del Farmaco, Università del Piemonte Orientale, Largo Donegani 2/3, 28100 Novara, Italy.

[c] Dep. of Physical Chemistry, University of Debrecen, Egyetem tér 1, H-4032 Debrecen, Hungary

[d] Bracco Imaging SpA, CRB Trieste, AREA Science Park, ed. Q – S.S. 14 Km 163.5 - 34149 Basovizza, TS, Italy.

[e] ITIS "A. Volta", Spalto Marengo 42, 15121 Alessandria, Italy

[f] Dip. di Scienze e Innovazione Tecnologica, Università del Piemonte Orientale, Via T. Michel 11, 15121 Alessandria, Italy. E-mail: mauro.botta@uniupo.it

[g] Universidade da Coruña, Centro de Interdisciplinar de Química e Bioloxía (CICA) and Departamento de Química, Facultade de Ciencias, 15071, A Coruña, Galicia, Spain

Table of contents

General

All chemicals were purchased from Merck, Alfa Aesar, or TCI Europe and were used without further purification. All aqueous solutions were prepared from ultrapure laboratory grade water (18 MΩ • cm) obtained from Millipore/MilliQ purification system. ^{1}H and ^{13}C NMR spectra were recorded at 400 MHz on a Bruker Avance Neo 400 spectrometer. Chemical shifts are reported in ppm with the protic impurities of the deuterated solvent as the internal reference. Mass spectra were obtained with a Thermo Finningan LCQ-Deca XP-PLUS ion trap spectrometer equipped with an electrospray source. High resolution mass spectra were registered on a ThermoScientific Q-Exactive Plus spectrometer. TLC were performed with silica gel (MN Kieselgel 60F254) and visualized by UV or sprayed with Dragendorff reagent or alkaline $KMnO_4$. Column chromatography was carried out on Macherey-Nagel Silica gel 60 (0.063-0.200 mm). HMF (**1**)[1] and *cis*-2,5-*bis*-(hydroxymethyl)tetrahydrofuran **(2)**[2] were prepared according to literature procedures, and spectroscopic data were consistent with those reported.

Synthetic procedures

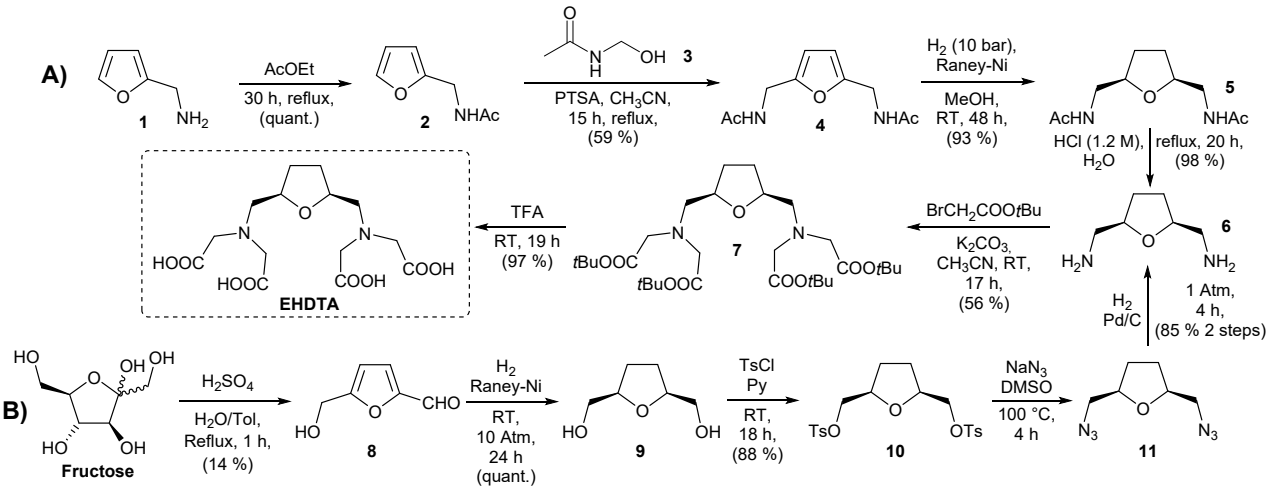

Synthesis of *cis*-2,5-*bis*-(hydroxymethyl)tetrahydrofuran ditosylate (10). Compound **9** (2.00 g, 15.2 mmol) was dissolved at room temperature in acetonitrile (10 mL). *p*-Toluensufonyl chloride (8.66 g, 45.6 mmol) and pyridine (15.6 g, 197.6 mmol) were sequentially added at room temperature, and the resulting reaction mixture was stirred at room temperature overnight. Water (10 mL) was added and the resulting suspension was filtered and washed with water and with cold ethanol. The residual solvent was removed by evaporation under reduced pressure, affording compound **10** (4.9 g, 88 %) as a white crystalline solid. ^{1}H NMR (400 MHz, $CDCl_3$, 298 K) δ 7.77 (d, J = 8.0 Hz, 4H), 7.34 (d, J = 8.0 Hz, 4H), 4.09 (p, J = 5.4 Hz, 2H), 3.96 – 3.89 (m, 4H), 2.45 (s, 6H), 2.02 – 1.89 (m, 2H), 1.76 – 1.66 (m, 2H) ppm. ^{13}C NMR (101 MHz, $CDCl_3$, 298 K) δ 145.1 (C), 132.9 (C), 130.1 (CH), 128.1 (CH), 77.1 (CH), 71.2 (CH_2), 27.6 (CH_2), 21.8 (CH_3) ppm.

Synthesis of *cis*-2,5-*bis*-(azidomethyl)tetrahydrofuran (11). Sodium azide (2.1 g, 32.4 mmol, 3 eq) was added at room temperature to a stirred solution of **10** (4 g, 10.8 mmol) in DMSO (10 mL). The resulting reaction mixture was stirred at 100 °C for 4 hours, checking periodically by TLC. Water was added and the resulting solution was extracted thrice with diethylether. The organic layers were combined and the solvent was reduced by evaporation under reduced pressure. Methanol was added and the diethylether was completely removed by evaporation under reduced pressure. One portion was completely dried to give 10 mg of **11** for NMR analysis. The rest of the solution was used for the next step without the removal of the methanol. ^{1}H NMR (400 MHz, $CDCl_3$, 298 K) δ 4.13 (p, J = 5.2 Hz, 2H), 3.40 (dd, J = 12.8/4.1 Hz, 2H), 3.29 (dd, J = 12.8/5.6 Hz, 2H), 2.10 – 1.94 (m, 2H), 1.84 – 1.71 (m, 2H) ppm. ^{13}C NMR (101 MHz, $CDCl_3$, 298 K) δ 78.8 (CH), 54.7 (CH_2), 28.6 (CH_2) ppm.

Synthesis of *cis*-2,5-*bis*-(aminomethyl)tetrahydrofuran (6). Palladium on charcoal (10 % w/w, 0.5 g) was added to the solution obtained in the previous step (compound **11** in methanol) and hydrogen was flowed in for 4 hours, checking periodically by TLC. The solution was filtered and the solvent was removed by evaporation under reduced pressure. The resulting oil was purified by gravity-flow chromatography on silica-gel column (petroleum ether/ethyl acetate 7:3), affording 1.18 g of **6** (1.18 g, 85 % from ditosylate) as a yellowish liquid. ^{1}H NMR (400 MHz, $CDCl_3$, 298 K) δ 3.85 (p, J = 5.3 Hz, 2H), 3.37 (s, 4H), 2.76 (dd, J = 13.1/3.7 Hz, 2H), 2.63 (dd, J = 13.1/7.0 Hz, 2H), 2.02 (br s, 4H), 1.94 – 1.85 (m, 2H), 1.59 – 1.47 (m, 2H) ppm. ^{13}C NMR (101 MHz, $CDCl_3$, 298 K) δ 80.9 (CH), 46.7 (CH_2), 28.5 (CH_2) ppm.

Synthesis of EHDTA-*t*Bu$_4$ (7). Compound **6** (600 mg, 4.6 mmol) was dissolved in acetonitrile (10 mL) at room temperature, and potassium carbonate (3.2 g, 23 mmol) was added. The resulting solution was cooled down to 0°C with an ice bath and *tert*-butyl bromoacetate (3.8 g, 19.3 mmol) was added dropwise. The resulting reaction mixture was allowed to warm to room temperature and stirred overnight. After checking by TLC, the solution was filtered and the solvent was removed by evaporation under reduced pressure. The crude product was purified by gravity-flow chromatography on silica-gel column (petroleum ether/ethyl acetate 8:2) affording EHDTA-*t*Bu$_4$ **7** (1.5 g, 56 %) as a yellowish oil. ^{1}H NMR (400 MHz, $CDCl_3$, 298 K) δ 4.00 – 3.93 (m, 2H), 3.51 (d, J = 17.3 Hz, 4H), 3.42 (d, J = 17.4 Hz, 4H), 2.87 (dd, J = 13.5/6.3 Hz, 2H), 2.71 (dd, J = 13.6/4.8 Hz, 2H), 1.93 – 1.85 (m, J = 4.3 Hz, 2H), 1.65 – 1.56 (m, 2H), 1.43 (s, 36H) ppm. ^{13}C NMR (101 MHz, $CDCl_3$, 298 K) δ 171.0 (C), 80.8 (C), 79.3 (CH), 59.0 (CH_2), 57.0 (CH_2), 29.3 (CH_2), 28.3 (CH_3) ppm. MS (ESI$^+$): m/z = 587.39 (100%, [M+H]$^+$). Calc. for $C_{30}H_{54}N_2O_9$+H$^+$: 587.39.

Synthesis of EHDTA. EHDTA-*t*Bu$_4$ **7** (1.0 g, 1.7 mmol) was dissolved at room temperature in trifluoroacetic acid (10 mL), and the resulting reaction mixture was stirred overnight at room temperature. Volatiles were removed by evaporation under reduced pressure and the product was purified by dissolution in MeOH and precipitation with diethyl ether. This procedure was repeated 2-3 times, affording **EHDTA** (600 mg, 97 %) as a white hygroscopic solid. ^{1}H NMR (400 MHz, D_2O, 298 K) δ 4.48 – 4.42 (m, 2H), 4.24 (d, J = 17.3 Hz, 4H), 4.18 (d, J = 17.2 Hz, 4H), 3.66 (d, J = 13.4 Hz, 2H), 3.45 (dd, J = 13.6/10.0 Hz, 2H), 2.23 – 2.16 (m, 2H), 1.74 – 1.66 (m, 2H) ppm. ^{13}C NMR (101 MHz, D_2O, 298 K) δ 168.6 (C), 74.8 (CH), 59.6 (CH_2), 55.6 (CH_2), 28.2 (CH_2) ppm. MS (ESI$^+$): m/z = 363.14 (100%, [M+H]$^+$). Calc. for $C_{14}H_{22}N_2O_9$+H$^+$: 363.14.

NMR spectra

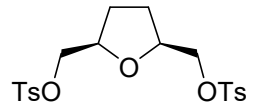

3

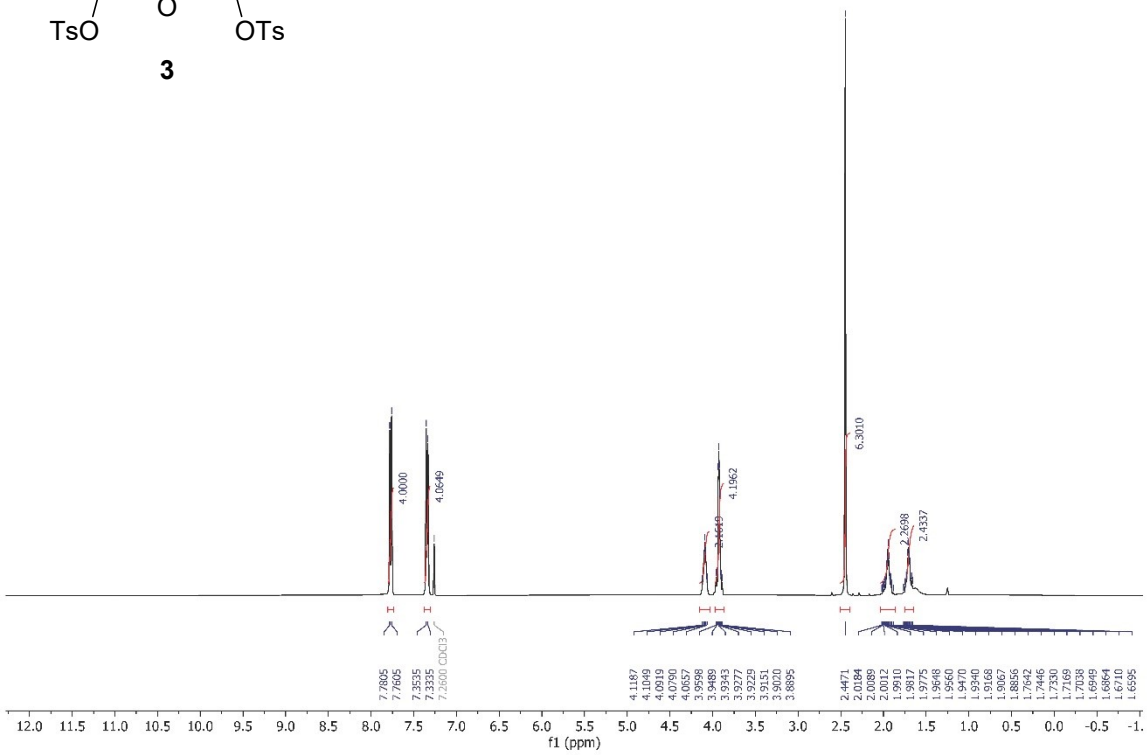

Figure S1. ^{1}H NMR spectrum of compound **3**.

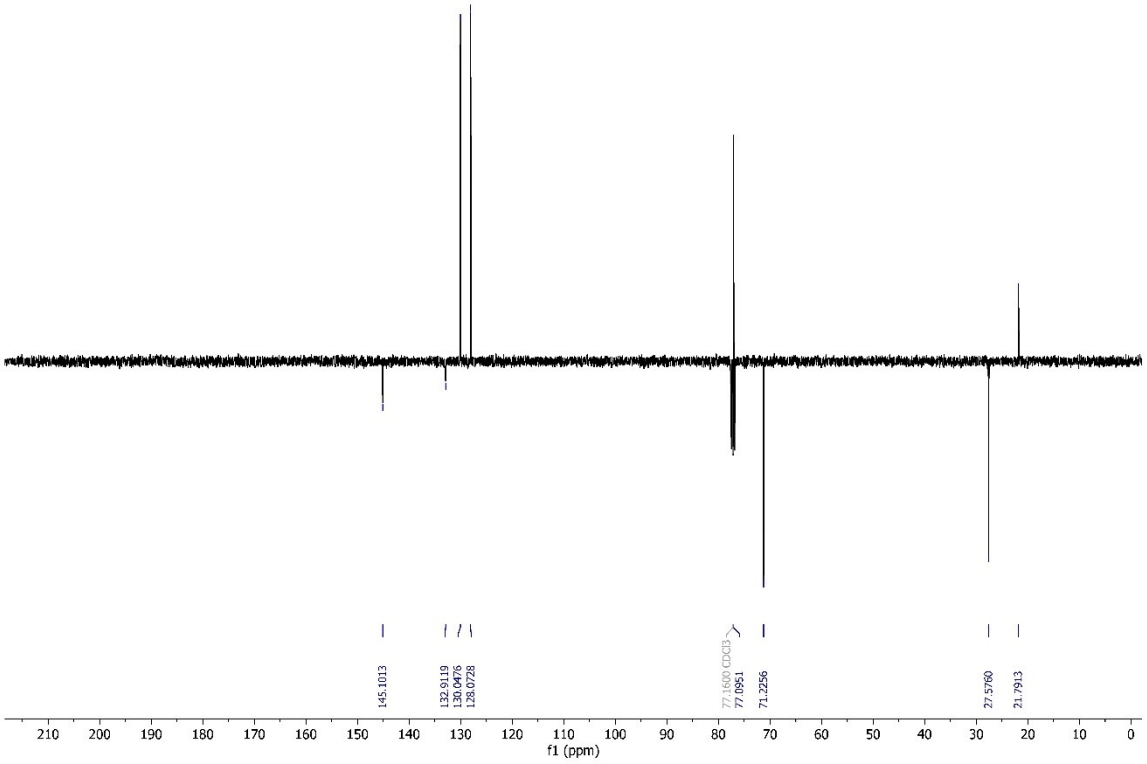

Figure S2. ^{13}C APT NMR spectrum of compound **3**.

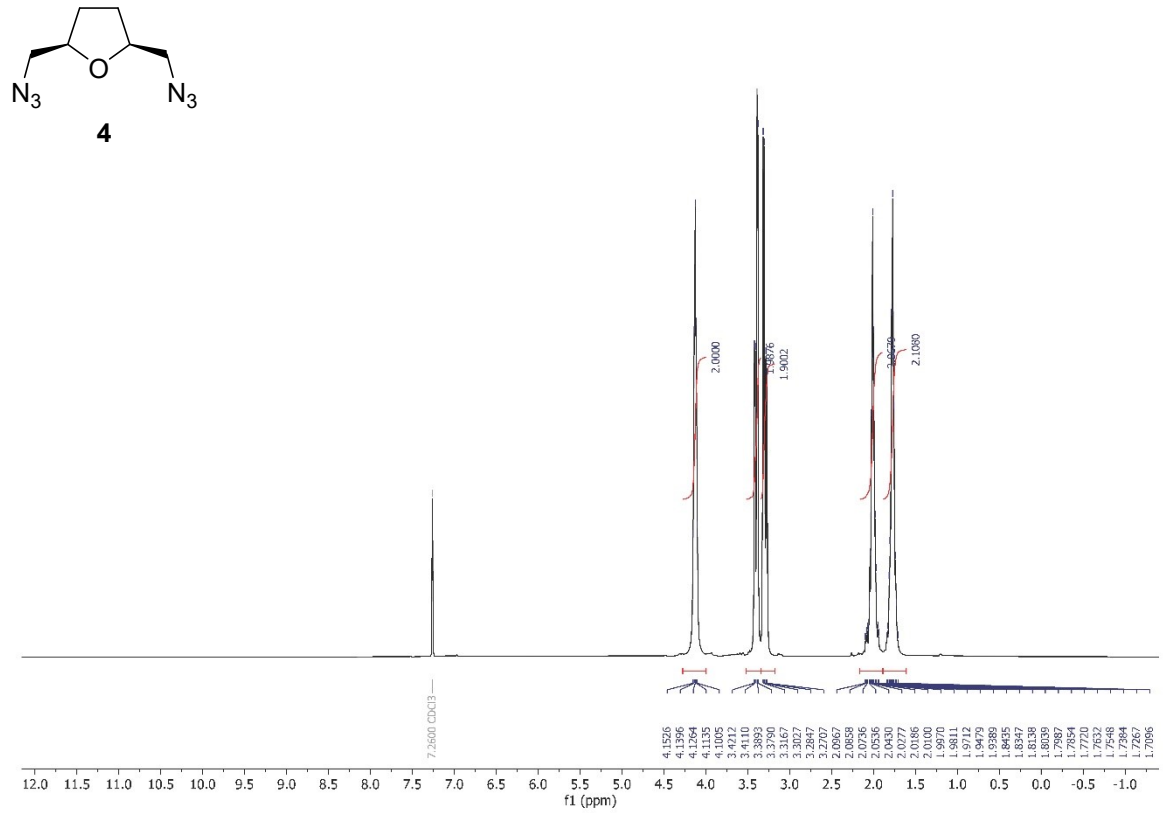

Figure S3. ^{1}H NMR spectrum of compound **4**.

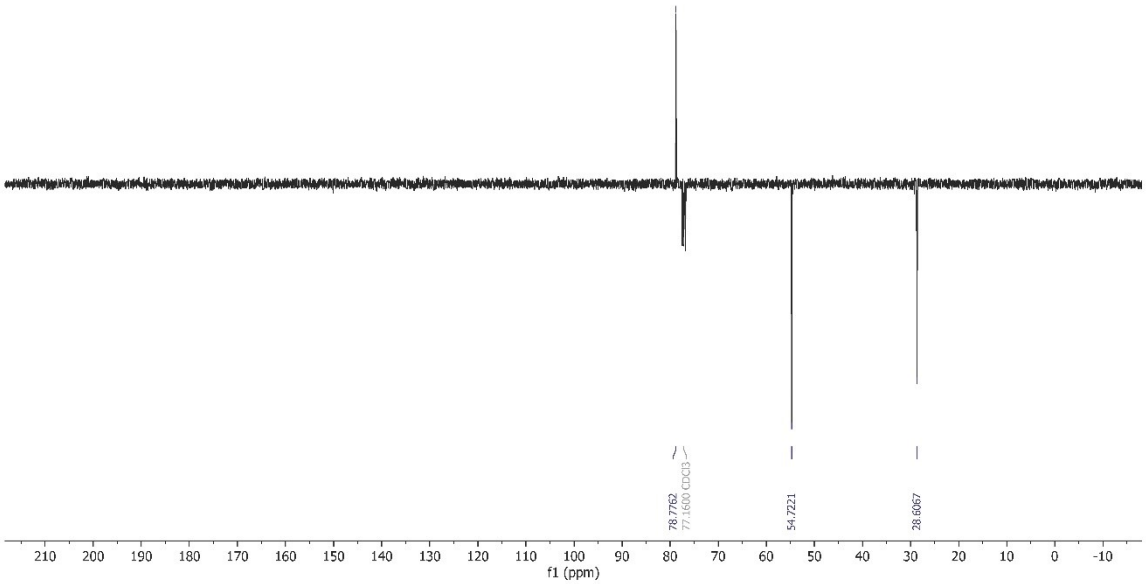

Figure S4. ^{13}C APT NMR spectrum of compound **4**.

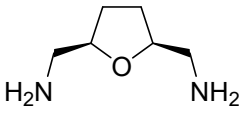

5

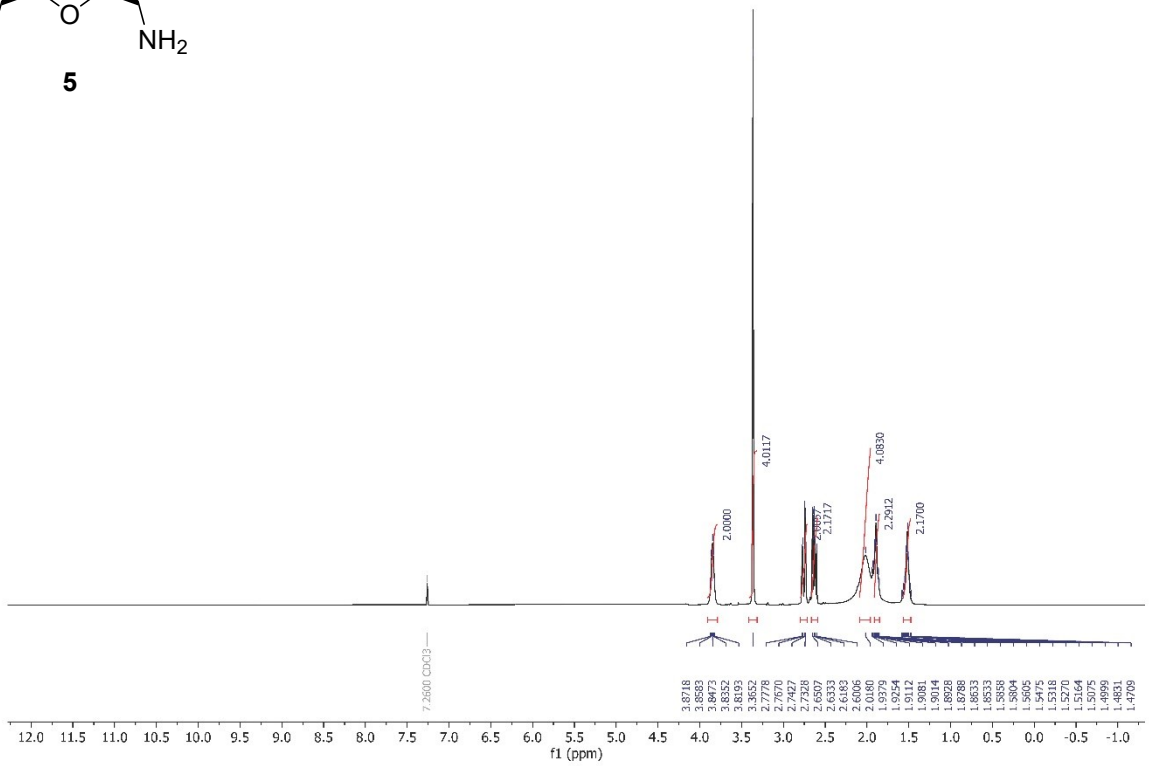

Figure S5. ^{1}H NMR spectrum of compound **5**.

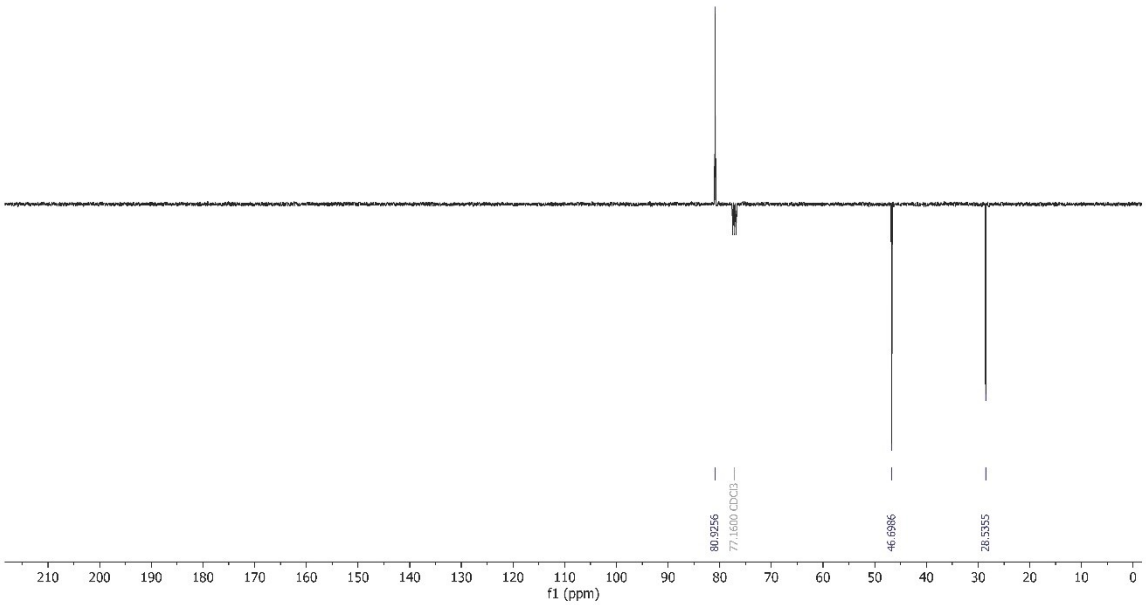

Figure S6. ^{13}C APT NMR spectrum of compound **5**.

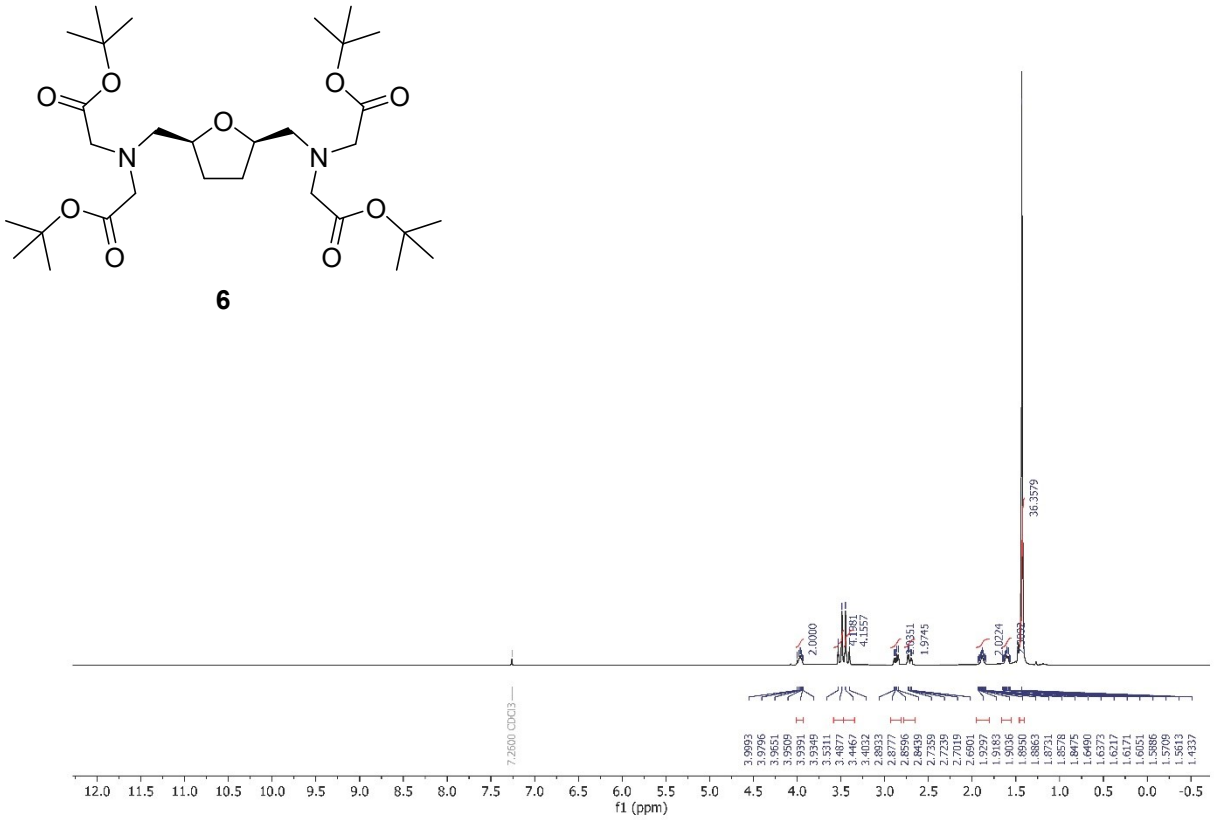

Figure S7. ^{1}H NMR spectrum of compound **6**.

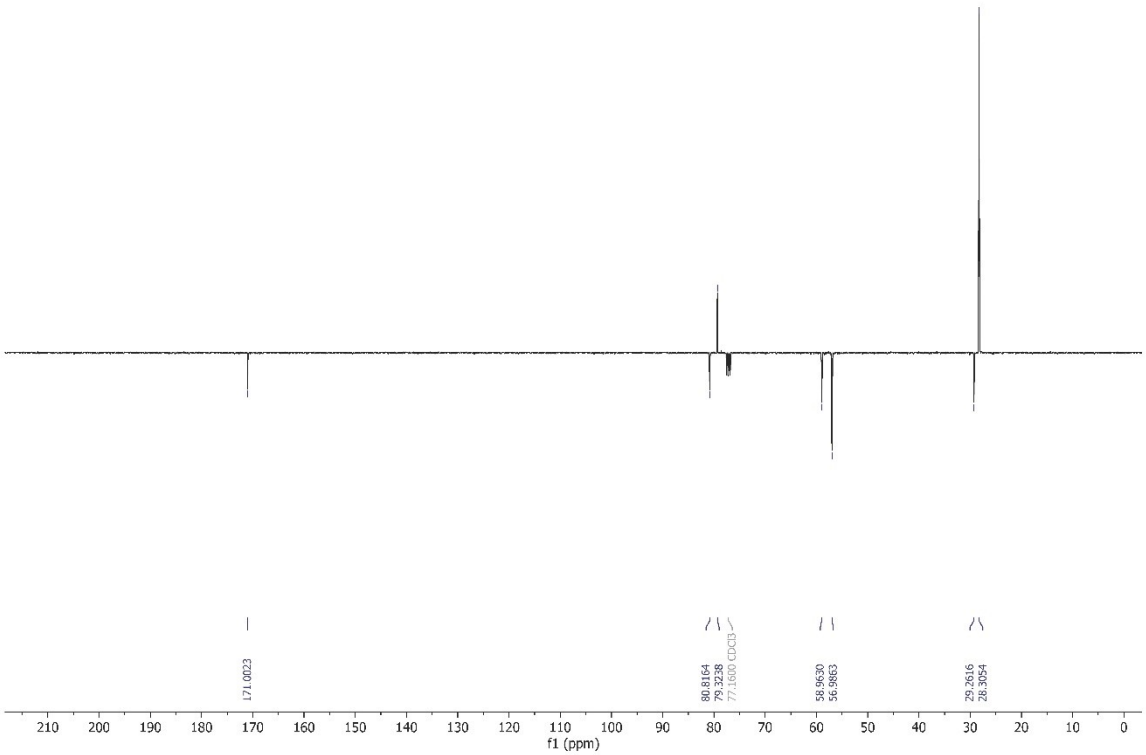

Figure S8. ^{13}C APT NMR spectrum of compound **6**.

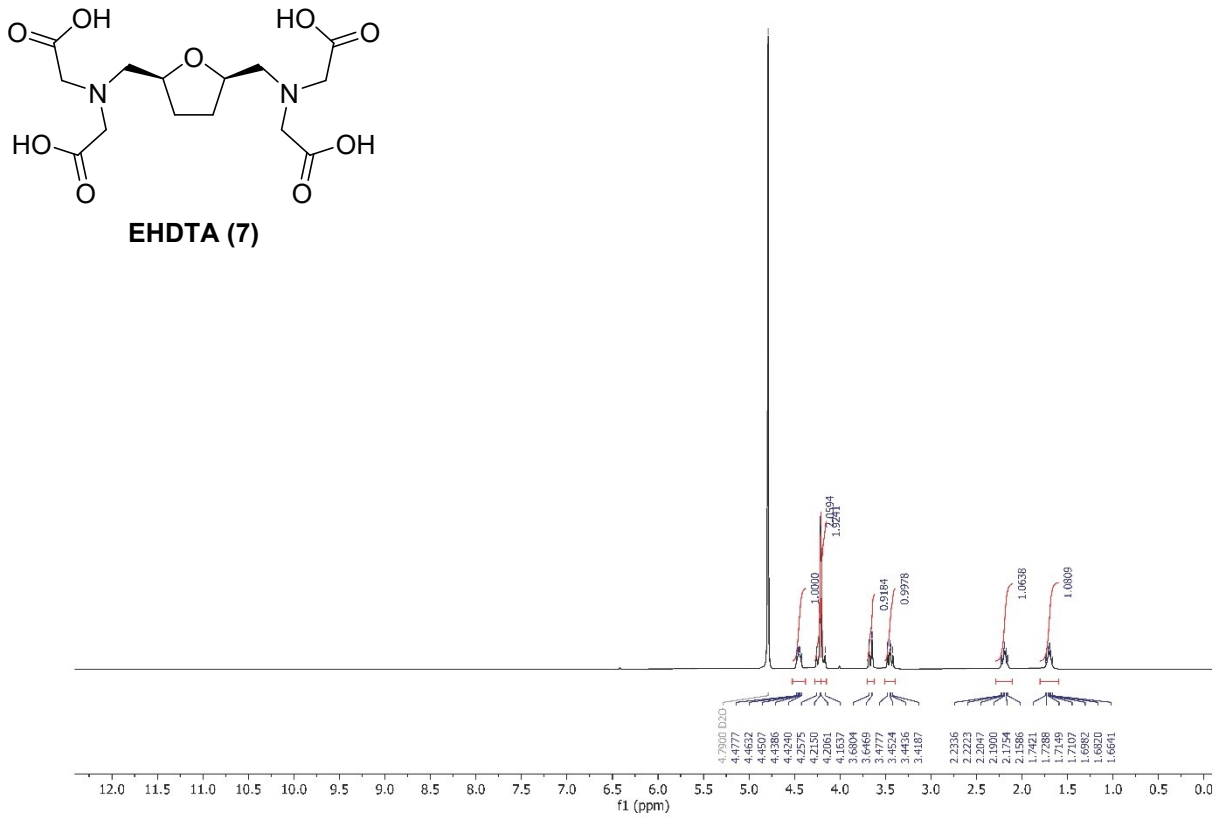

Figure S9. ^{1}H NMR spectrum of compound **7**.

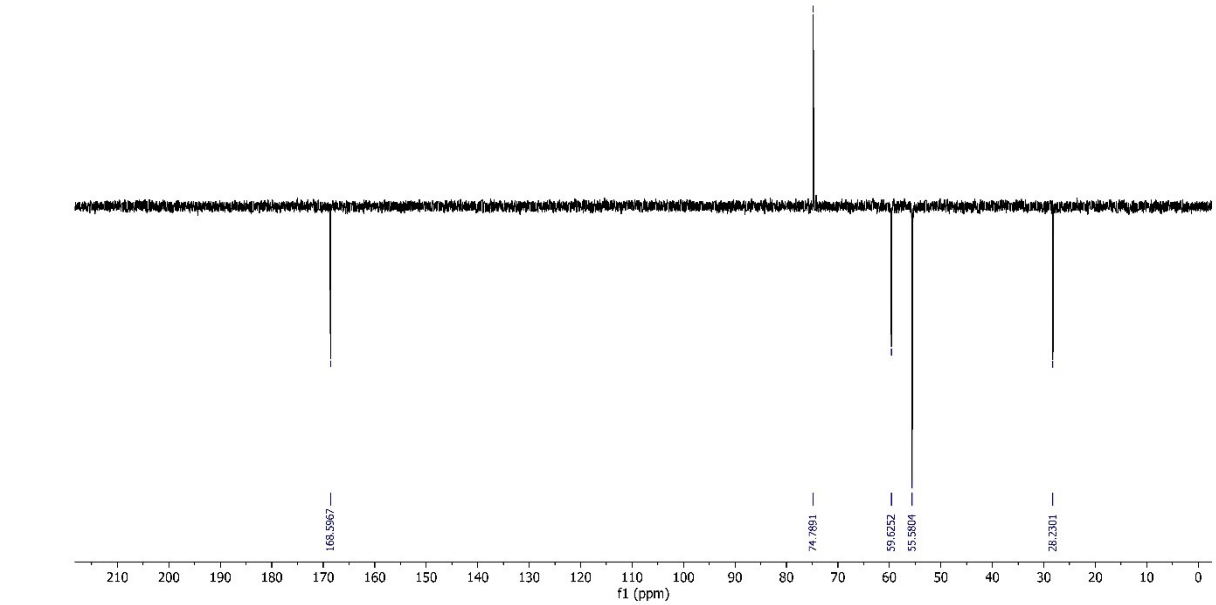

Figure S10. ^{13}C APT NMR spectrum of compound **7**.

HRMS spectra

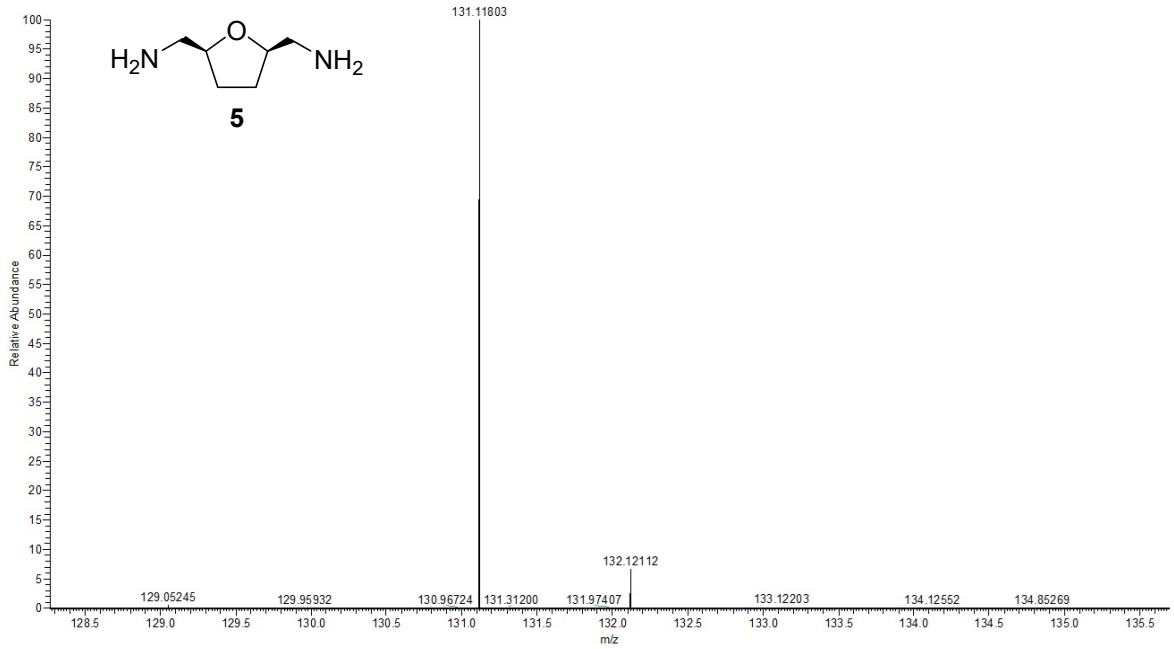

Figure S11. HRMS spectrum of compound **5**.

Thermodynamic studies

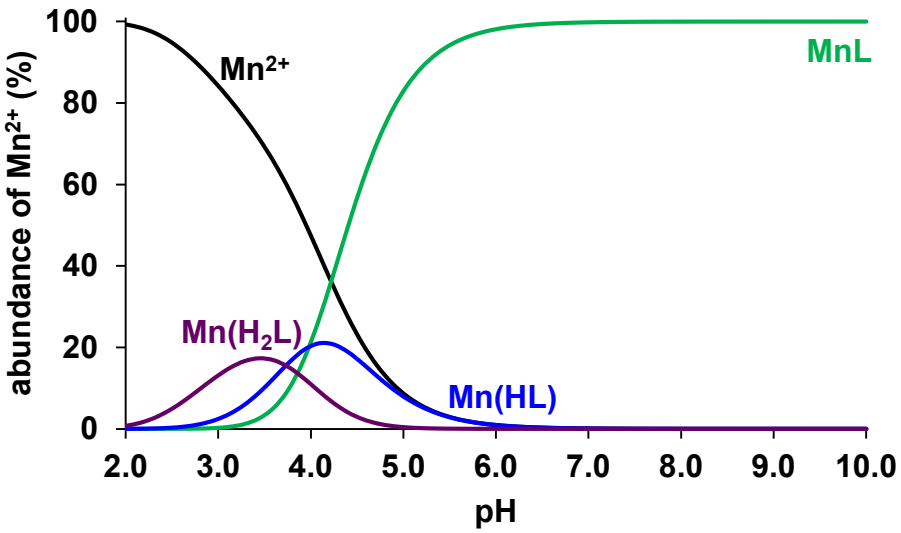

Figure S12. Species distribution of Mn^{2+} - EHDTA system ([Mn^{2+}]=[L]=1.0 mM, 0.1 M KCl, 25°C)

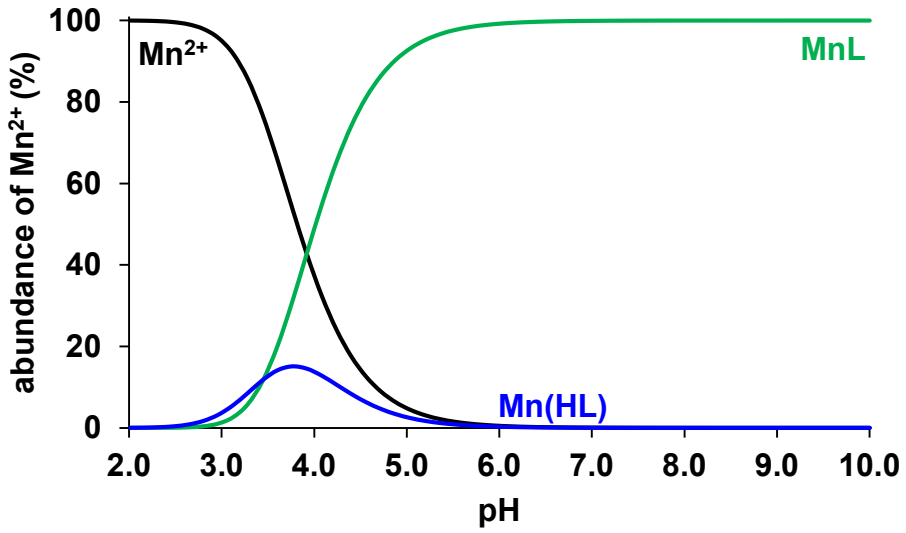

Figure S13. Species distribution of Mn^{2+} - OBETA system ([Mn^{2+}]=[L]=1.0 mM, 0.1 M KCl, 25°C)

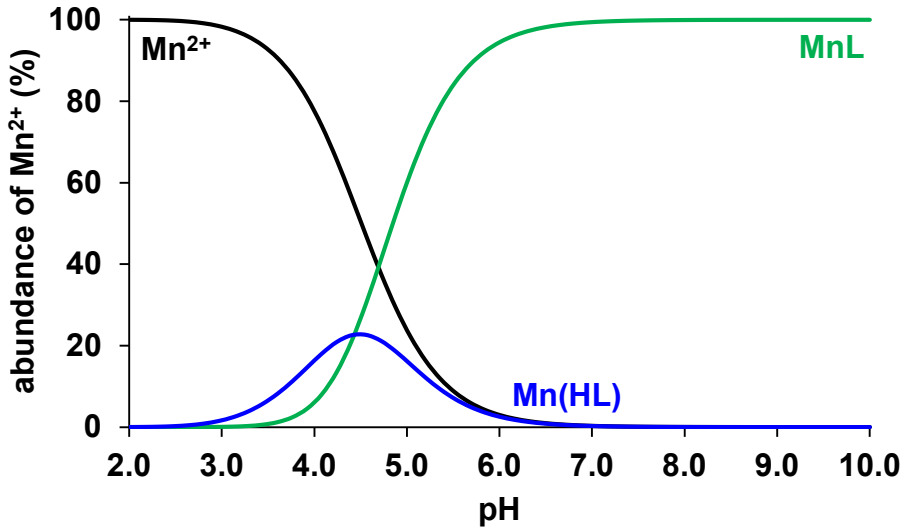

Figure S14. Species distribution of Mn^{2+} - EGTA system ([Mn^{2+}]=[L]=1.0 mM, 0.1 M KCl, 25°C)

Kinetic studies

The kinetic inertness of the $[Mn(EHDTA)]^{2-}$ and $[Mn(OBETA)]^{2-}$ complexes have been evaluated by following the transmetallation reactions between the Mn(II) complexes and Cu^{2+} with spectrophotometry in the presence of Cu^{2+} excess (Eq. (S1)).

$$MnL + Cu^{2+} \rightleftharpoons CuL + Mn^{2+} \qquad (S1)$$

Rates of the transmetallation reactions have been determined in the presence of 10 – 40 fold Cu^{2+} excess in the pH range 3.3 – 4.9 ([MnL]=0.1 mM, [Cu^{2+}]=1.0 – 4.0 mM, 0.15 M NaCl, 25°C). In the presence of large Cu^{2+} excess the transmetallation can be regarded as a pseudo-first-order process and the rate of reactions can be expressed with the Eq. (S2).

$$-\frac{d[MnL]_t}{dt} = k_d[MnL]_t \qquad (S2)$$

where k_d is a pseudo-first-order rate constant and $[MnL]_{tot}$ is the total concentration of Mn(II) complex. The pseudo-first-order rate constants (k_d) for the transmetallation reactions of $[Mn(EHDTA)]^{2-}$ and $[Mn(OBETA)]^{2-}$ with Cu^{2+} are plotted as a function of pH, $[H^+]$ and $[Cu^{2+}]$ in Figures S15 – S18.

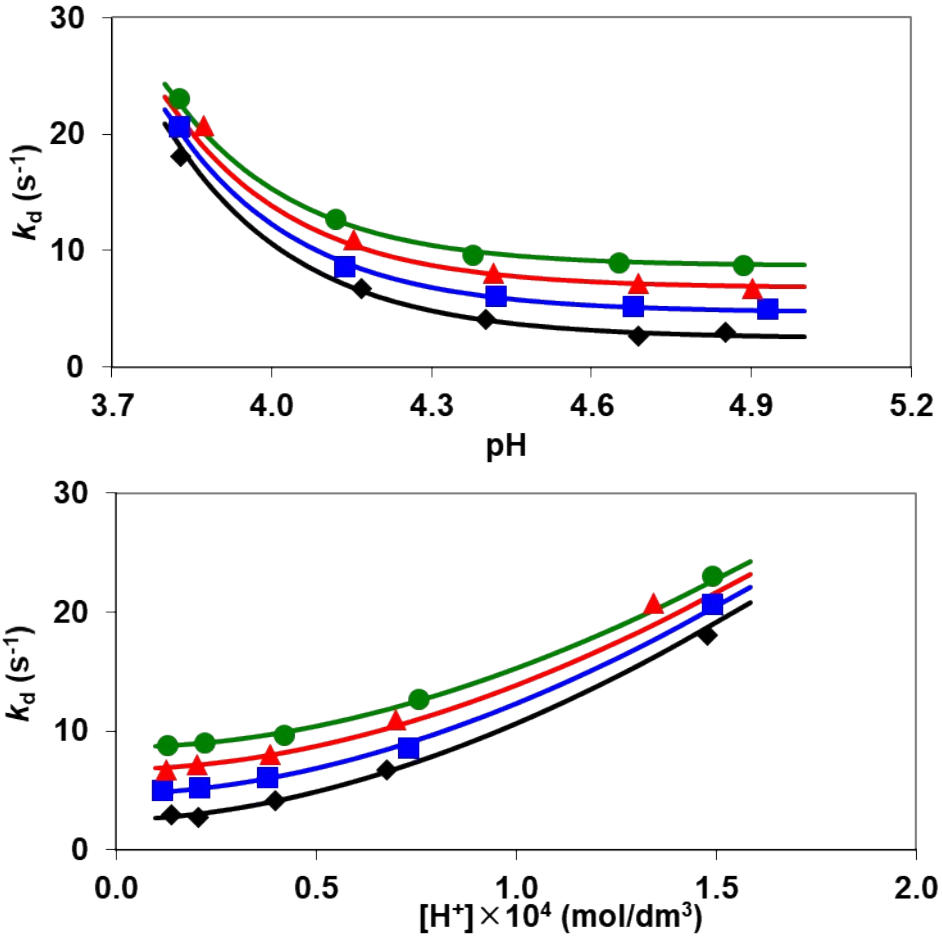

Figure S15. Pseudo-first order rate constants (k_d) characterize the transmetallation reactions of $[Mn(OBETA)]^{2-}$ with Cu^{2+} as a function of pH and $[H^+]$ ([MnL)] = 0.1 mM, $[Cu^{2+}]$ = 1.0 (🕘), 2.0 (■), 3.0 (□) and 4.0 mM (●) (20 mM NMP, 0.15 M NaCl, 25 °C).

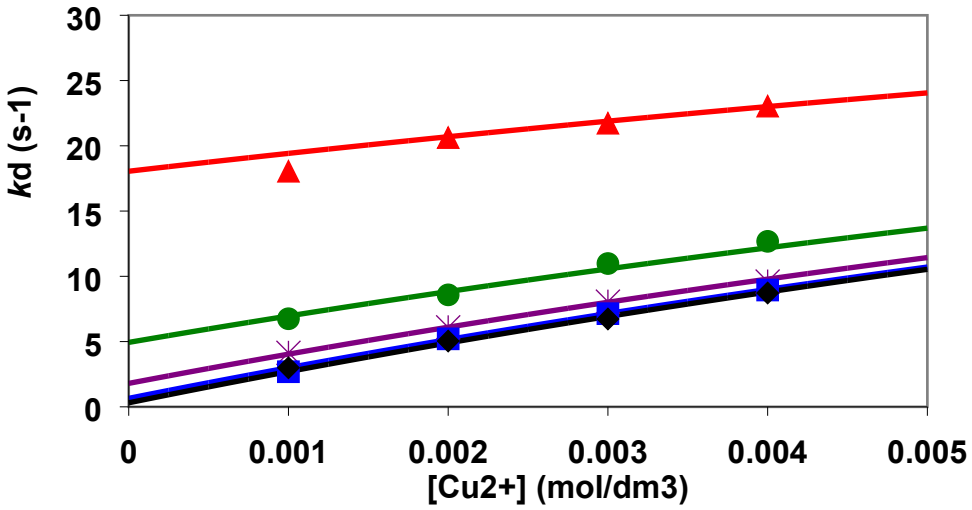

Figure S16. Pseudo-first order rate constants (k_d) characterize the transmetallation reactions of $[Mn(OBETA)]^{2-}$ with Cu^{2+} as a function of $[Cu^{2+}]$ ([MnL)] = 0.1 mM, pH= 4.89 (🕘), 4.68 (■), 4.40 (⋎), 4.14 (●) and 3.84 (□) (20 mM NMP, 0.15 M NaCl, 25 °C).

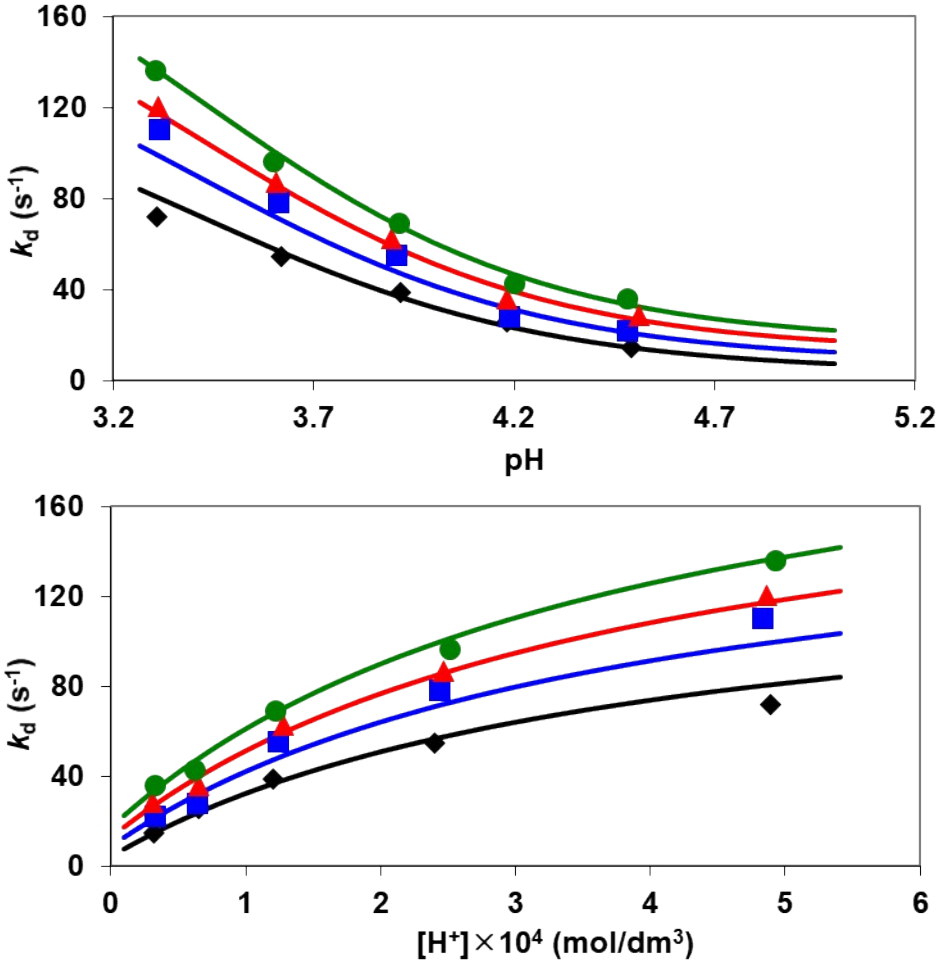

Figure S17. Pseudo-first order rate constants (k_d) characterize the transmetallation reactions of $[Mn(EHDTA)]^{2-}$ with Cu^{2+} as a function of pH and $[H^+]$ ([MnL] = 0.1 mM, $[Cu^{2+}]$ = 1.0 (🕘), 2.0 (■), 3.0 (□) and 4.0 mM (●) ([DMP]=[NMP]=0.01 M, 0.15 M NaCl, 25 °C).

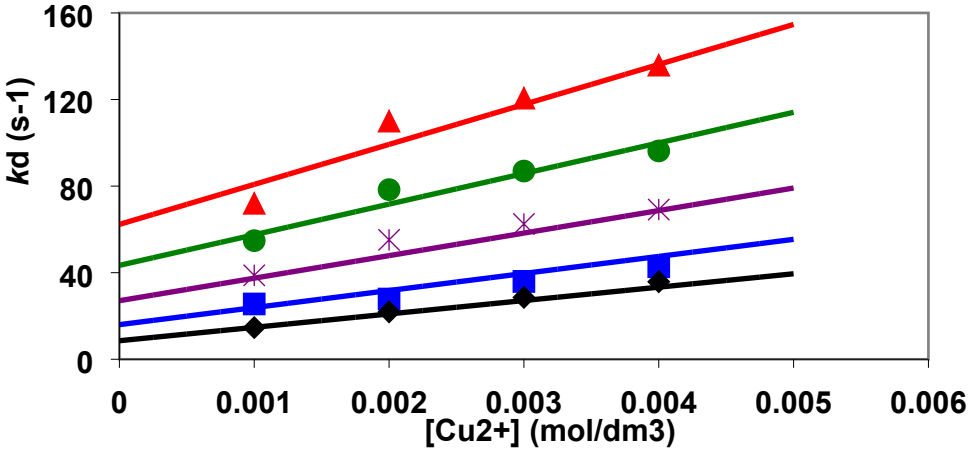

Figure S18. Pseudo-first order rate constants (k_d) characterize the transmetallation reactions of $[Mn(EHDTA)]^{2-}$ with Cu^{2+} as a function of $[Cu^{2+}]$ ([MnL] = 0.1 mM, pH= 4.49 (🕘), 4.19 (■), 3.91 (✳), 3.61 (●) and 3.31 (□) ([DMP]=[NMP]=0.01 M, 0.15 M NaCl, 25 °C)

The kinetic data presented in Figures S15 – S18 indicates that the k_d values characterizing the transmetallation reaction of $[Mn(EHDTA)]^{2-}$ and $[Mn(OBETA)]^{2-}$ with Cu^{2+} increase with increase of the $[H^+]$ and $[Cu^{2+}]$. The transmetallation reactions of Mn(II) complexes takes place by the slow rate determining dissociation followed by a fast reaction between the free ligand and the exchanging metal ions.[3,4] The dependence of k_d on the $[H^+]$ can be expressed as a first- and second-order function of $[H^+]$ which indicates that the exchange can take place by proton independent (k_0, Eq. (S3)) and proton assisted ($k_{Mn(HL)}$ and $k^H_{Mn(HL)}$, Eqs. (S5) and (S6)) pathways. The proton assisted dissociations of Mn(II) complexes can be explained by the equilibrium formation of a protonated Mn(HL) species (Eq. (S4)), which can slowly dissociate to the free Mn^{2+} ion and the ligand in spontaneous and proton assisted reactions.

$$MnL \xrightarrow{k_0} Mn^{2+} + L \qquad (S3)$$

$K_{Mn(HL)}$

$$MnL + H^+ \rightleftharpoons Mn(HL) \qquad (S4)$$

$$K_{Mn(HL)} = \frac{[Mn(HL)]}{[MnL][H^+]}$$

$$Mn(HL) \xrightarrow{k_{Mn(HL)}} Mn^{2+} + HL \qquad (S5)$$

$$Mn(HL) + H^+ \xrightarrow{k^H_{Mn(HL)}} Mn^{2+} + H_2L \qquad (S6)$$

k_d rate constants also increase with the increase of $[Cu^{2+}]$. Similar behaviours have been identified for the transmetallation reactions of $[Mn(EDTA)]^{2-}$, $[Mn(CDTA)]^{2-}$ and $[Mn(EGTA)]^{2-}$ complexes with Cu^{2+} ions.[3] According to the kinetic data, the presence of large Cu^{2+} excess results in the formation of heterodinuclear Mn(L)Cu intermediate ($K_{Mn(L)Cu}$, Eq. (S7)) which can dissociate by the slow transfer of the functional groups from the Mn^{2+} to the exchanging Cu^{2+} ion ($k_{Mn(L)Cu}$, Eq. (S8)) leading the release of the Mn^{2+} ion and the formation of the corresponding CuL complex.

$$MnL + Cu^{2+} \overset{K_{Mn(L)Cu}}{\rightleftharpoons} [Mn(L)Cu] \qquad (S7)$$

$$K_{Mn(L)Cu} = \frac{[Mn(L)Cu]}{[MnL][Cu^{2+}]}$$

$$[Mn(L)Cu] \xrightarrow{k_{Mn(L)Cu}} Mn^{2+} + CuL \qquad (S8)$$

By taking into account all the possible pathways, the rate of the transmetallation of $[Mn(EHDTA)]^{2-}$ and $[Mn(OBETA)]^{2-}$ complexes can be expressed by Eq. (S9), where the [Mn(HL)] and [Mn(L)Cu] are the concentrations of the monoprotonated and the heterodinuclear complexes, respectively.

$$-\frac{[MnL]_t}{dt} = k_0[MnL] + k_{Mn(HL)}[Mn(HL)] + k^H_{Mn(HL)}[Mn(HL)][H^+] + k_{Mn(L)Cu}[Mn(L)Cu] \qquad (S9)$$

Considering the equations defining the protonation constant of the MnL species (Eq. (S4)) and the stability constant of the hetero-dinuclear Mn(L)Cu complex (Eq. (S7)), Eq. (S9) can be expressed as follows:

$$-\frac{[MnL]_t}{dt} = k_0[MnL] + k_{Mn(HL)}K_{Mn(HL)}[MnL][H^+] + k^H_{Mn(HL)}K_{Mn(HL)}[MnL][H^+]^2 + k_{Mn(L)Cu}K_{Mn(L)Cu}[MnL][Cu^{2+}] \qquad (S10)$$

In the presence of large Cu^{2+} excess the total concentration of the Mn(II) complex is given by Eqs. (S11 and S12).

$$[MnL]_{tot}=[MnL]+[Mn(HL)]+[Mn(L)Cu]=[MnL](1+K_{Mn(HL)}[H^+]+K_{Mn(L)Cu}[Cu^{2+}]) \quad (S11)$$

$$\frac{[MnL]_{tot}}{1+K_{Mn(HL)}[H^+]+K_{Mn(L)Cu}[Cu^{2+}]}=[MnL] \quad (S12)$$

Combination of Eqs. (S2), (S10) and (S12) leads to Eq. (S13).

$$k_d[MnL]_{tot}=\frac{k_0+k_{Mn(HL)}K_{Mn(HL)}[H^+]+k^{H}_{Mn(HL)}K_{Mn(HL)}[H^+]^2+k_{Mn(L)Cu}K_{Mn(L)Cu}[Cu^{2+}]}{1+K_{Mn(HL)}[H^+]+K_{Mn(L)Cu}[Cu^{2+}]}[MnL]_{tot} \quad (S13)$$

By the substitution of $k_{Mn(HL)}\times K_{Mn(HL)}$, $k^{H}_{Mn(HL)}\times K_{Mn(HL)}$ and $k_{Mn(L)Cu}\times K_{Mn(L)Cu}$ terms with k_1, k_2 and k_3^{Cu} parameters in the numerator of Eq. (S13), the pseudo-first-order rate constant (k_d) can be expressed as follows:

$$k_d=\frac{k_0+k_1[H^+]+k_2[H^+]^2+k_3^{Cu}[Cu^{2+}]}{1+K_{Mn(HL)}[H^+]+K_{Mn(L)Cu}[Cu^{2+}]} \quad (S14)$$

where k_0, k_1, k_2 and k_3^{Cu} parameters are the rate constants characterise the spontaneous, proton- and metal-assisted dissociation of the $[Mn(EHDTA)]^{2-}$ and $[Mn(OBETA)]^{2-}$ complexes, respectively. The rate and equilibrium constants that characterise the transmetalation reaction of $[Mn(EHDTA)]^{2-}$ and $[Mn(OBETA)]^{2-}$ complexes were calculated by fitting the k_d values presented in Figures S15 – S18 to Eq. (S14).

^{1}H and ^{17}O NMR relaxometric data

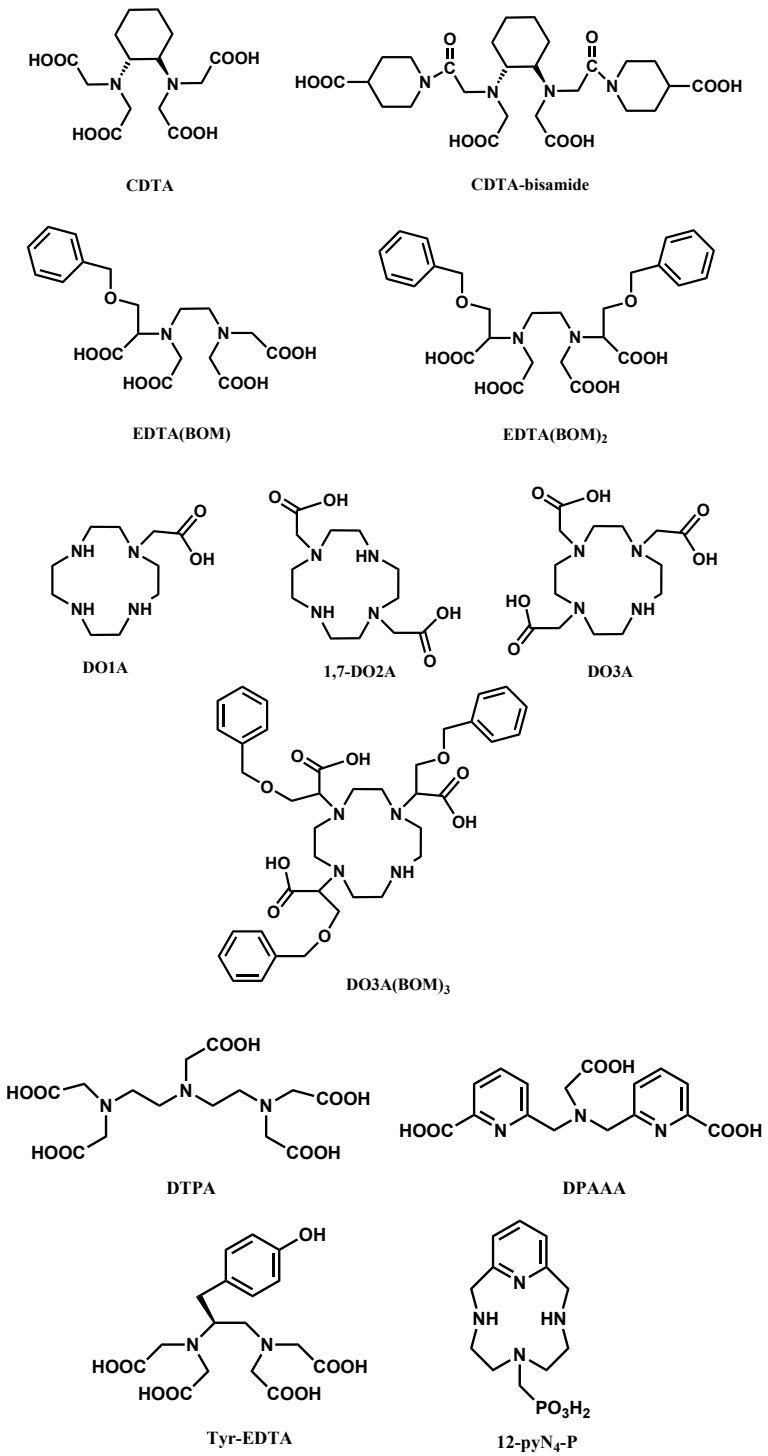

Scheme S1. Ligands discussed in Figure 2.

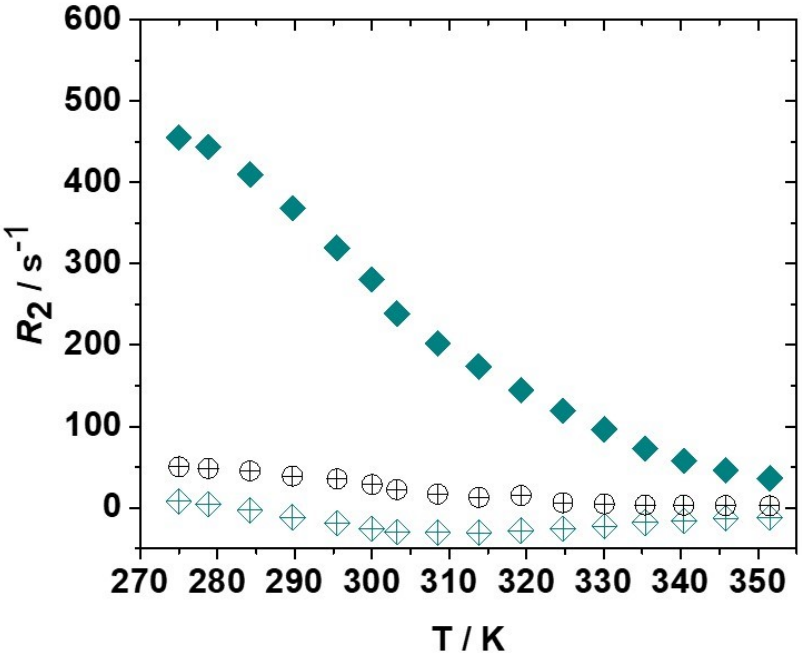

Figure S19. Temperature dependence of the transverse ^{17}O water relaxation rate (R_2) measured at 67.8 MHz (11.74 T) of $[Mn(EGTA)]^{2-}$ (◊), $[Mn(EHDTA)]^{2-}$ (○) and $[Mn(OBETA)]^{2-}$ (♦).

Solution structure and dynamic processes of the $[Zn(EHDTA)]^{2-}$, $[Zn(OBETA)]^{2-}$ and $[Zn(EGTA)]^{2-}$.

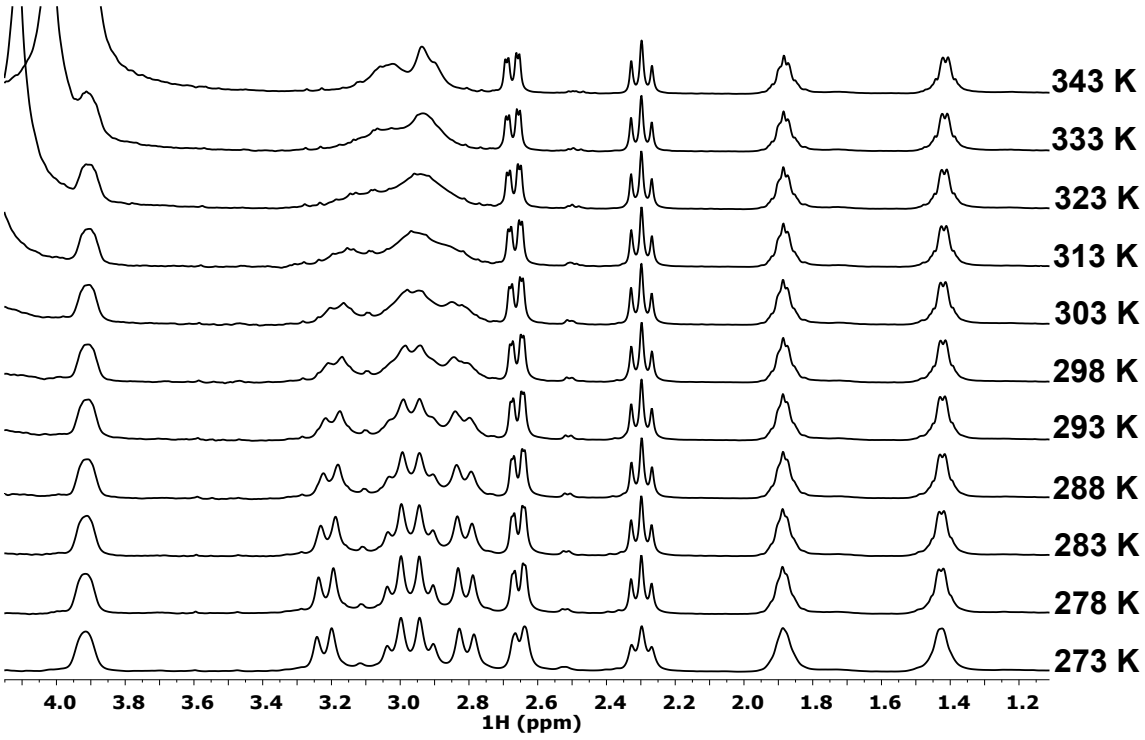

Figure S20. VT-^{1}H NMR spectra of $[Zn(EHDTA)]^{2-}$ ([ZnL]=50 mM, pH=7.10, 9.4 T, D_2O)

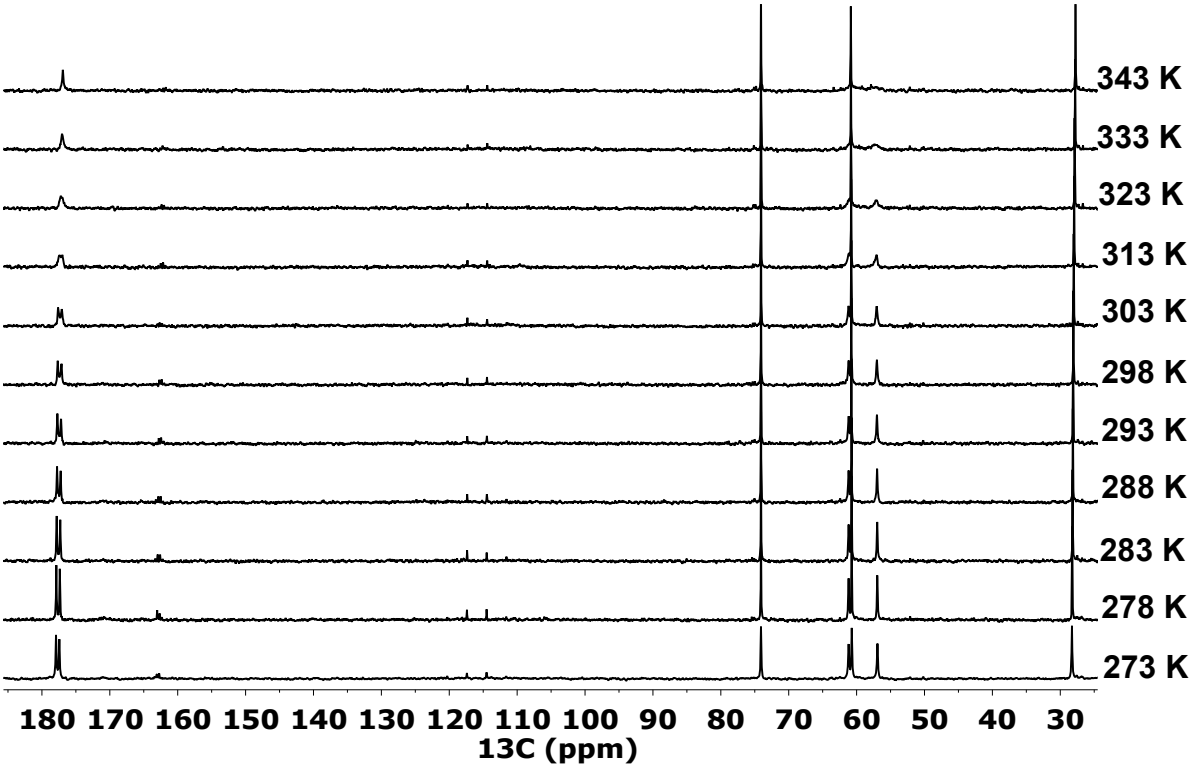

Figure S21. VT-^{13}C NMR spectra of $[Zn(EHDTA)]^{2-}$ ([ZnL]=50 mM, pH=7.01, 9.4 T, D_2O)

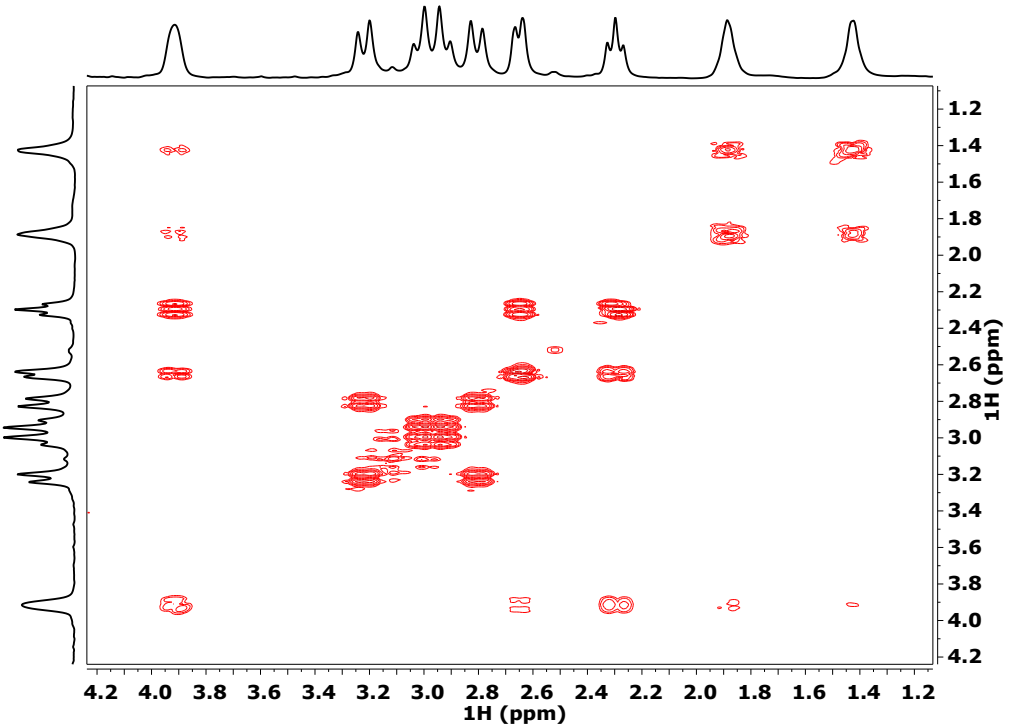

Figure S22. ^{1}H – ^{1}H COSY spectra of $[Zn(EHDTA)]^{2-}$ complex ([ZnL]=50 mM, pH=7.10, D_2O, 9.4 T, 273 K)

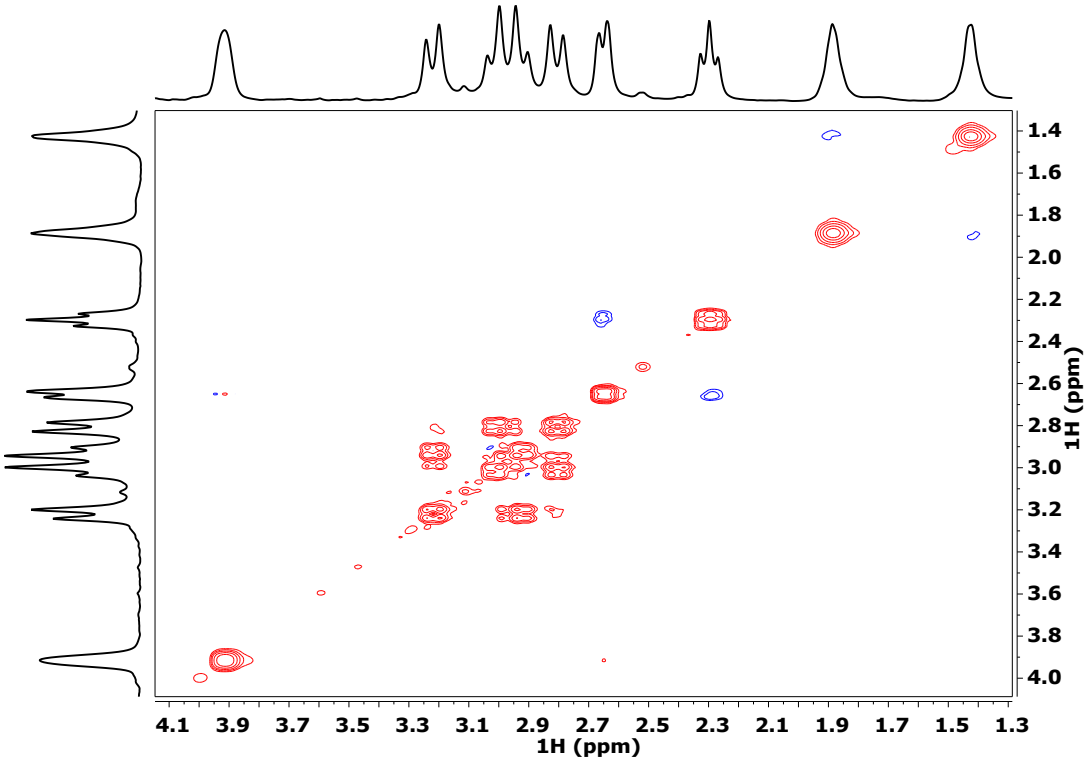

Figure S23. $^{1}H - {}^{1}H$ EXSY spectra of $[Zn(EHDTA)]^{2-}$ complex ([ZnL]=50 mM, pH=7.10, D_2O, D8=200 ms 9.4 T, 298 K)

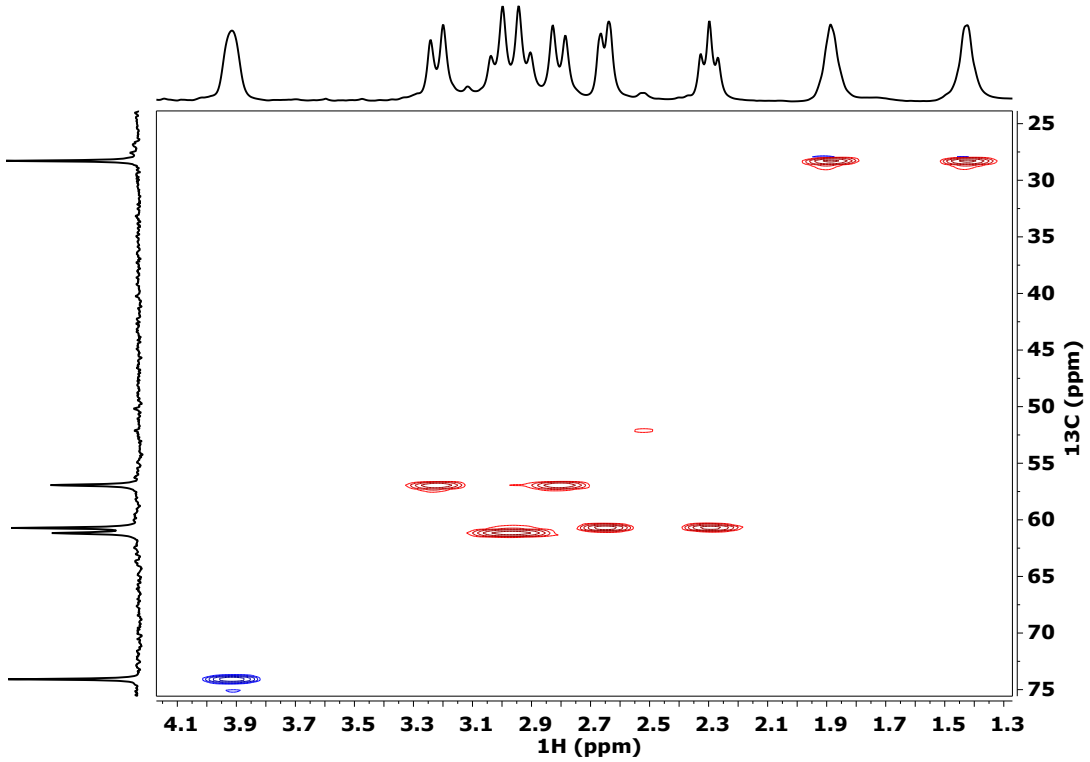

Figure S24. $^{1}H - {}^{13}C$ HSQC spectra of of $[Zn(EHDTA)]^{2-}$ complex ([ZnL]=50 mM, pH=7.10, D_2O, 9.4 T, 274 K)

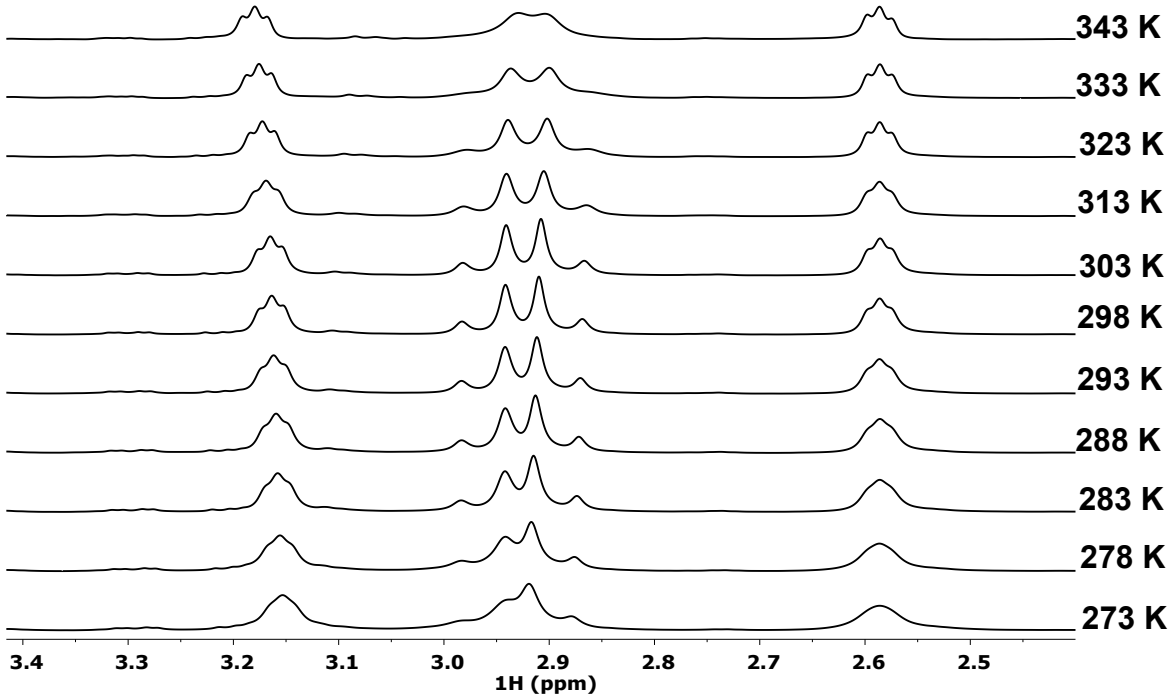

Figure S25. VT-^{1}H NMR spectra of $[Zn(OBETA)]^{2-}$ ([ZnL]=50 mM, pH=7.01, 9.4 T, D_2O)

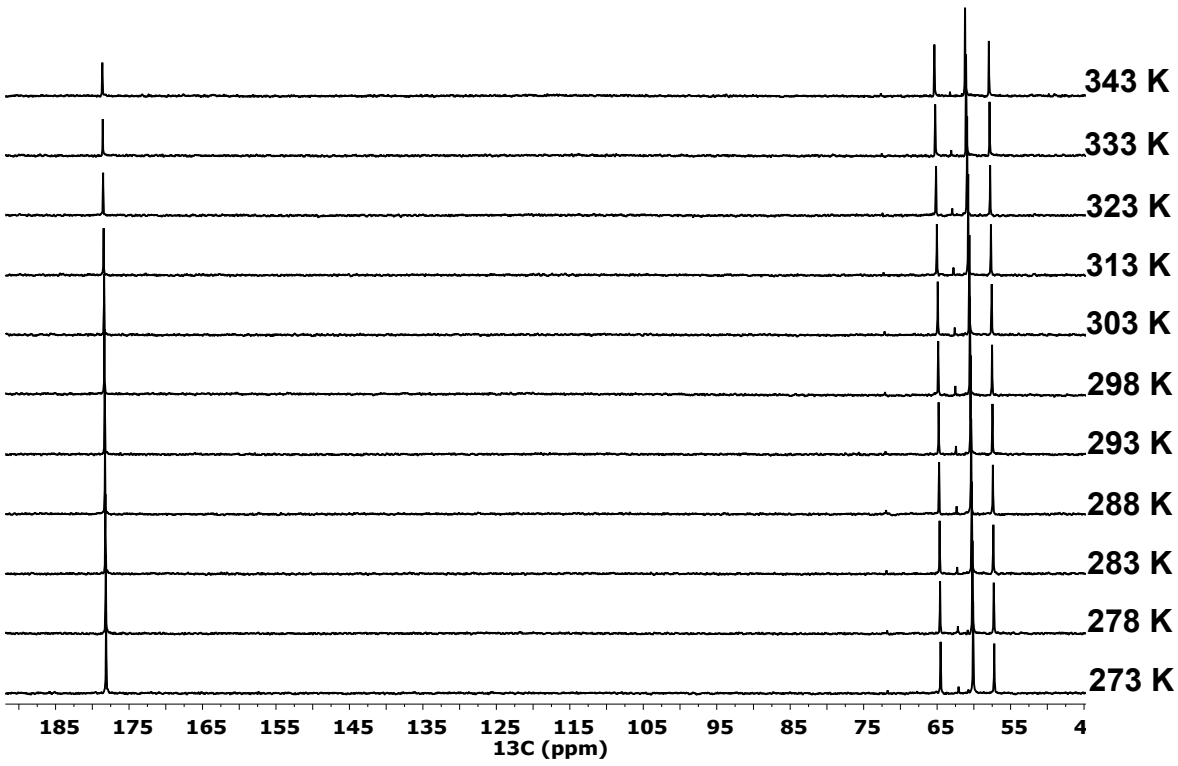

Figure S26. VT-^{13}C NMR spectra of $[Zn(OBETA)]^{2-}$ ([ZnL]=50 mM, pH=7.01, 9.4 T, D_2O)

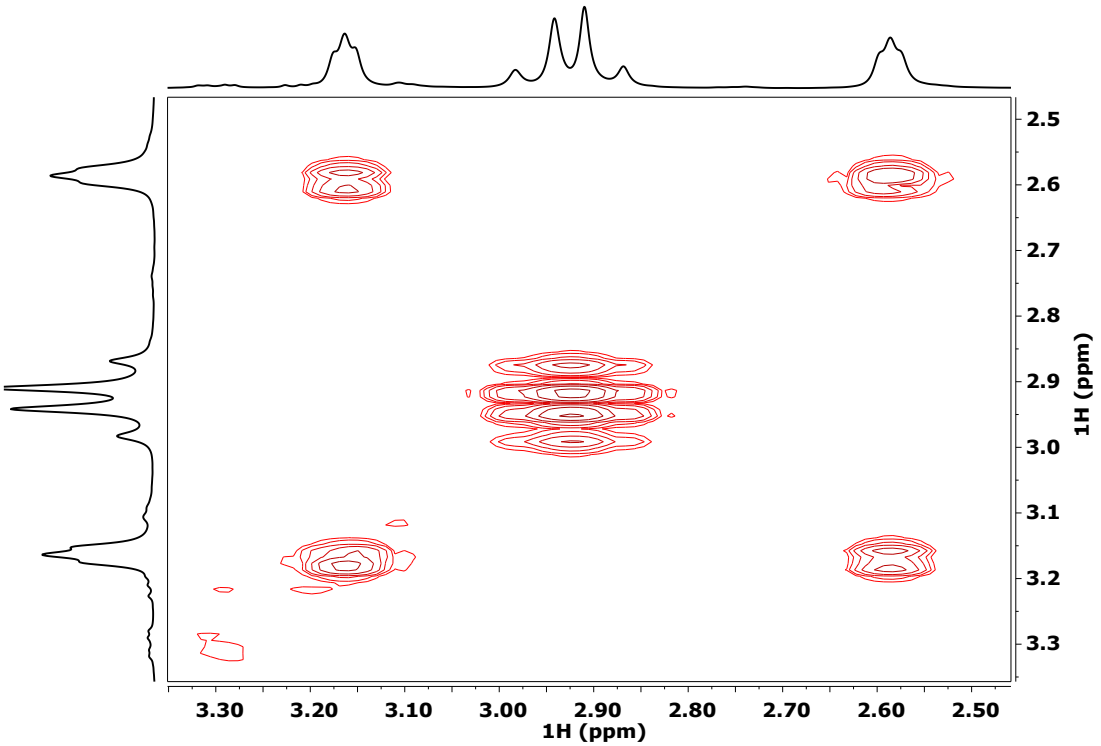

Figure S27. $^{1}H - {}^{1}H$ COSY spectra of $[Zn(OBETA)]^{2-}$ complex ([ZnL]=50 mM, pH=7.01, D_2O, 9.4 T, 298 K)

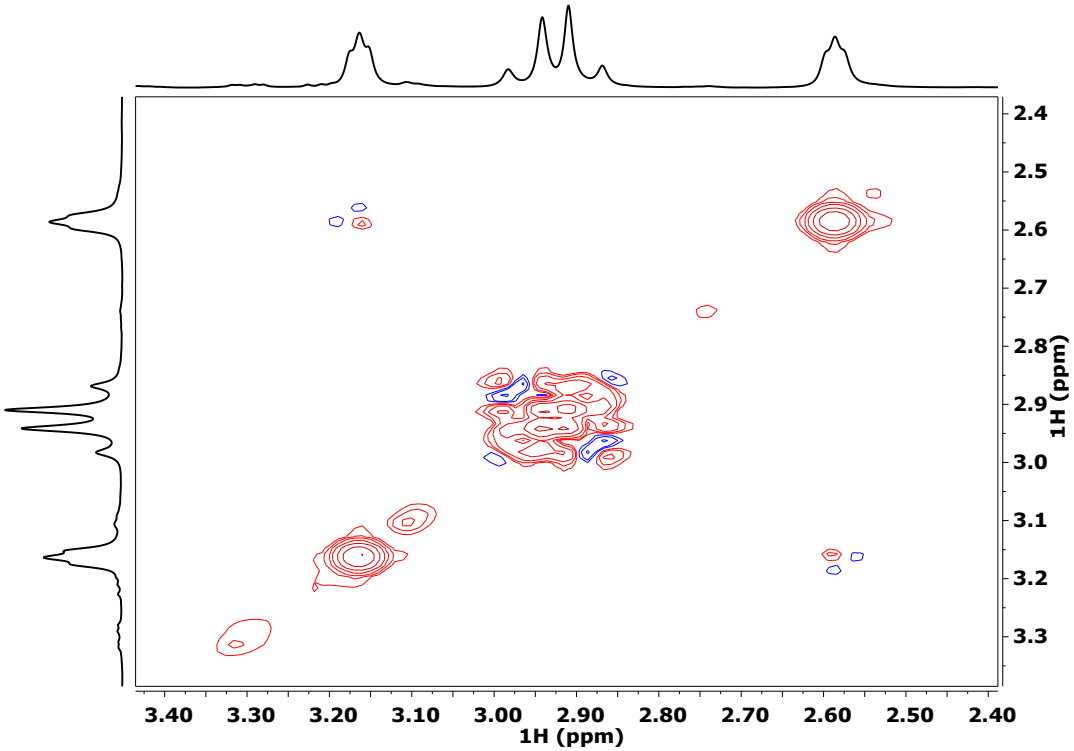

Figure S28. $^{1}H - {}^{1}H$ EXSY spectra of $[Zn(OBETA)]^{2-}$ complex ([ZnL]=50 mM, pH=7.01, D_2O, D8=200 ms 9.4 T, 298 K)

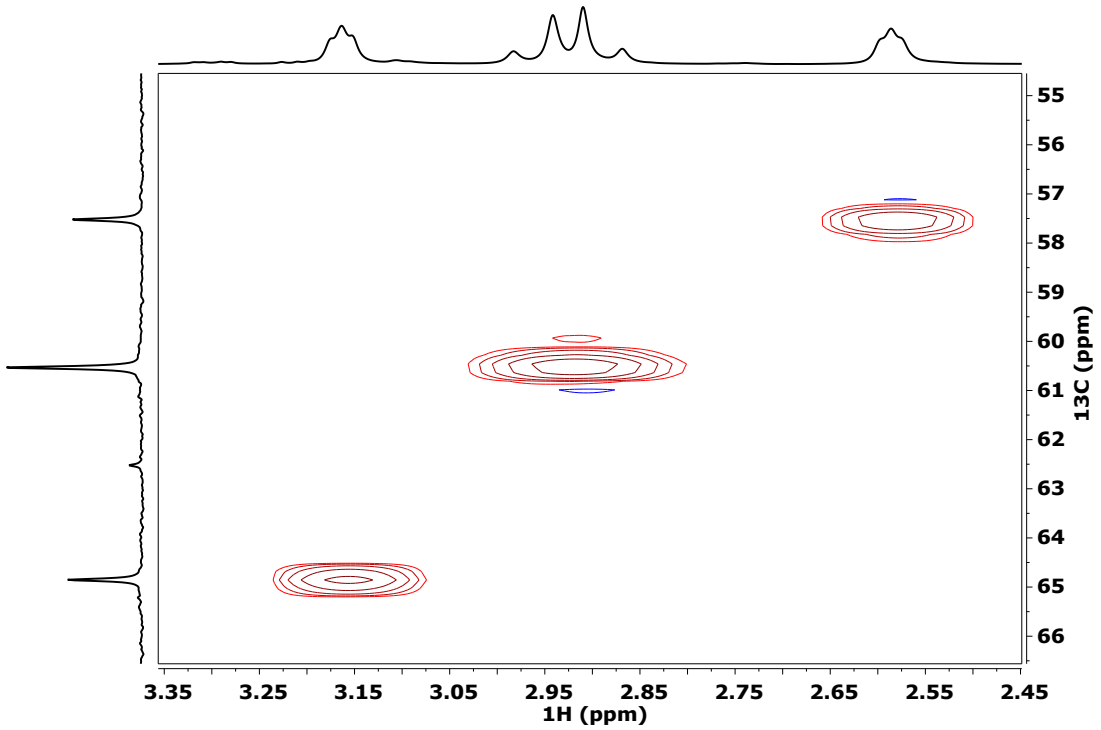

Figure S29. ^{1}H – ^{13}C HSQC spectra of of $[Zn(OBETA)]^{2-}$ complex ([ZnL]=50 mM, pH=7.01, D_2O, 9.4 T, 298 K)

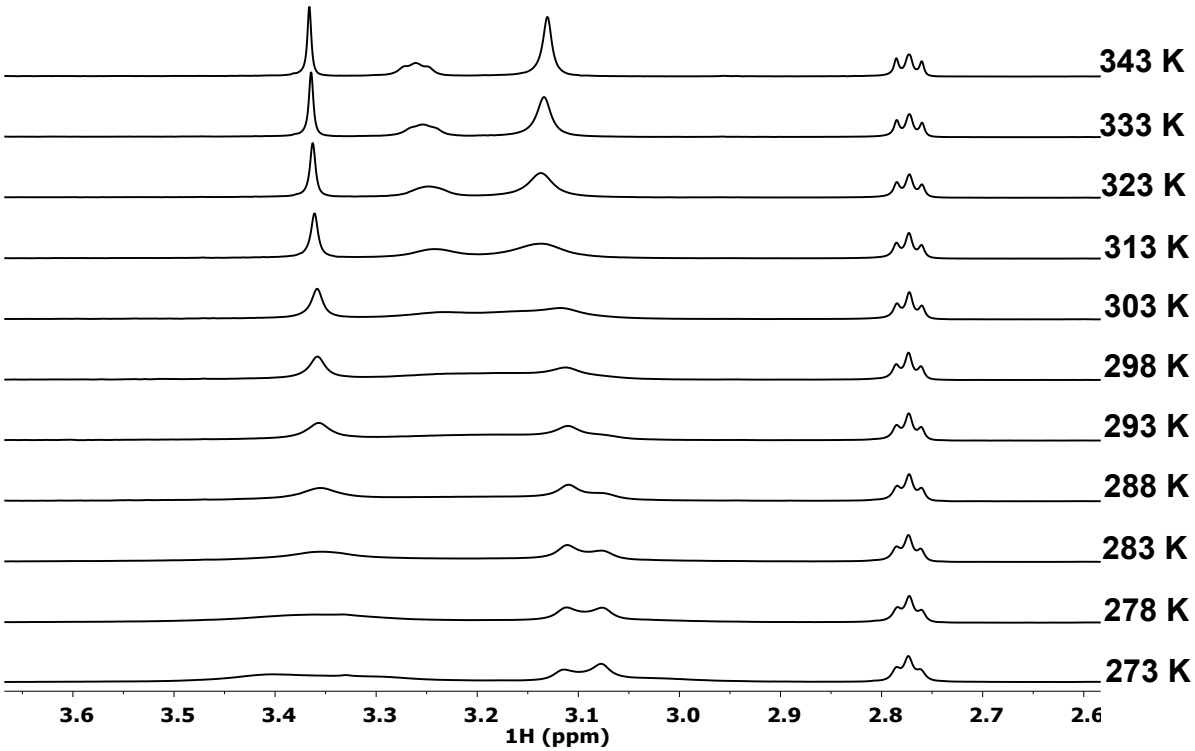

Figure S30. VT-^{1}H NMR spectra of $[Zn(EGTA)]^{2-}$ ([ZnL]=50 mM, pH=7.04, 9.4 T, D_2O)

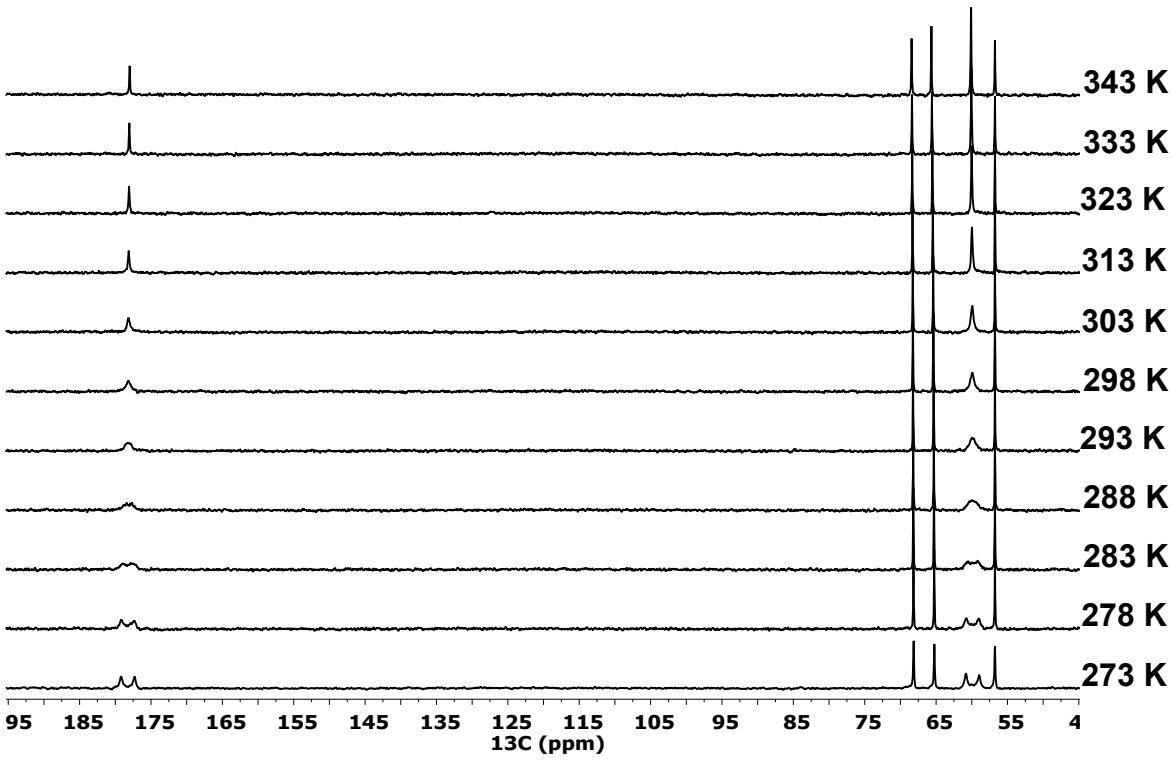

Figure S31. VT-^{13}C NMR spectra of $[Zn(EGTA)]^{2-}$ ([ZnL]=50 mM, pH=7.04, 9.4 T, D_2O)

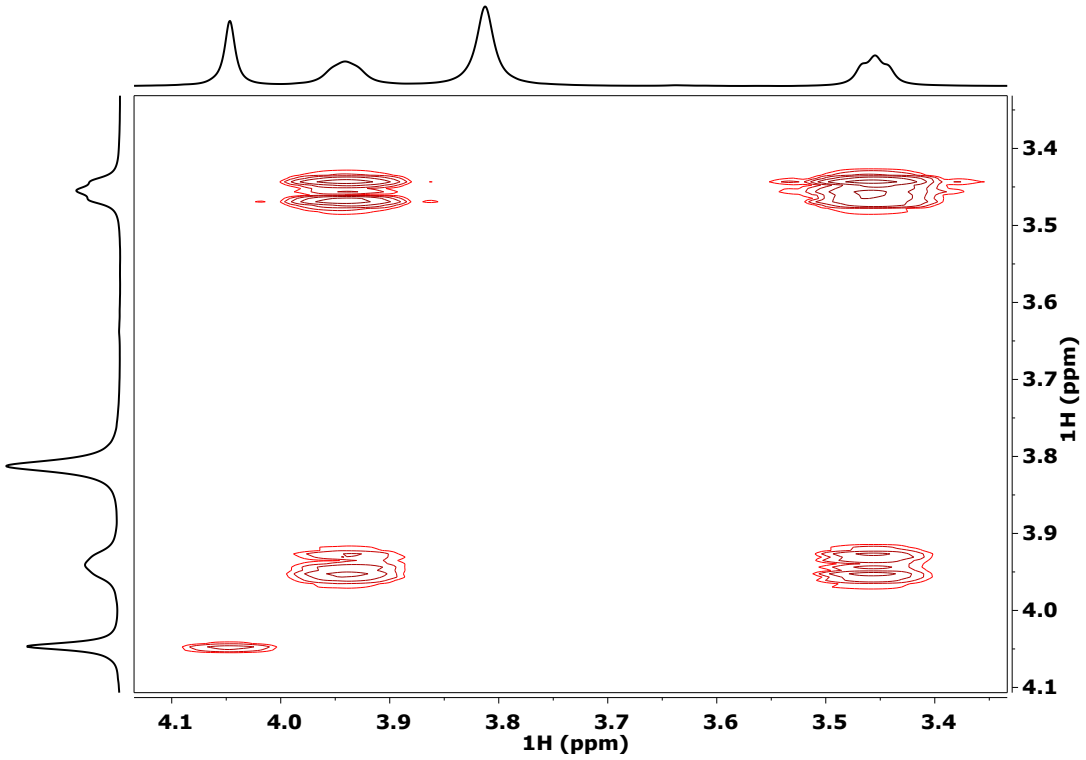

Figure S32. ^{1}H – ^{1}H COSY spectra of $[Zn(EGTA)]^{2-}$ complex ([ZnL]=50 mM, pH=7.04, D_2O, 9.4 T, 343 K)

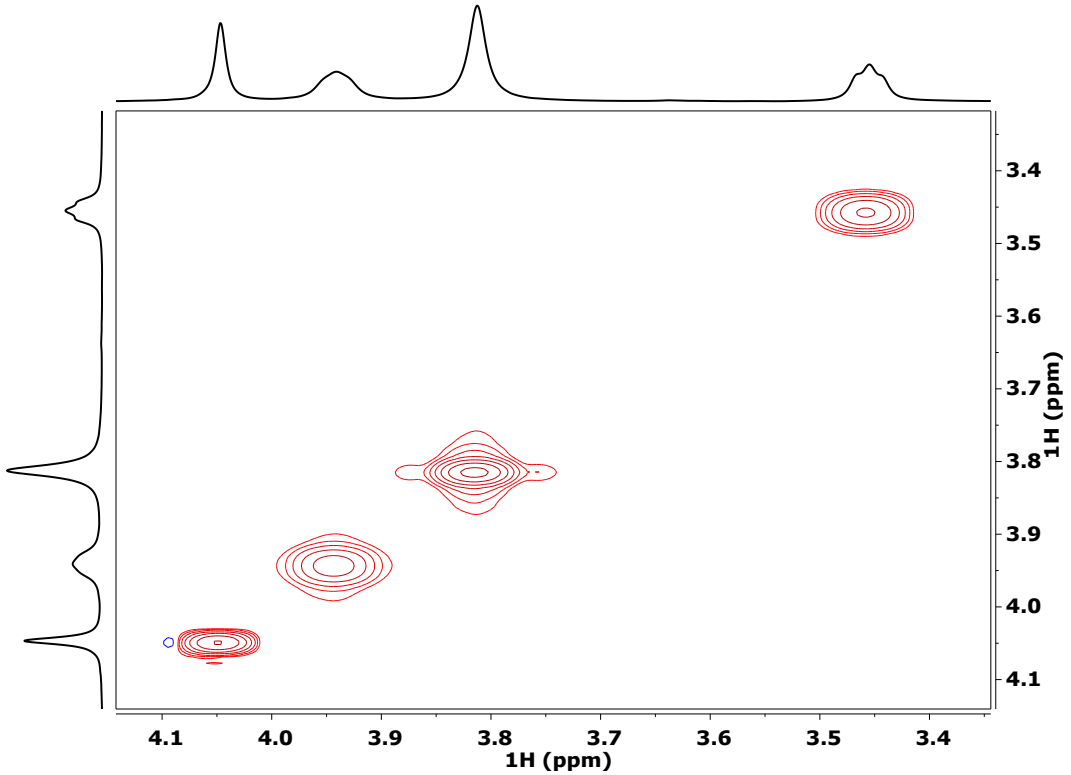

Figure S33. $^{1}H - {}^{1}H$ EXSY spectra of $[Zn(EGTA)]^{2-}$ complex ([ZnL]=50 mM, pH=7.04, D_2O, D8=200 ms 9.4 T, 343 K)

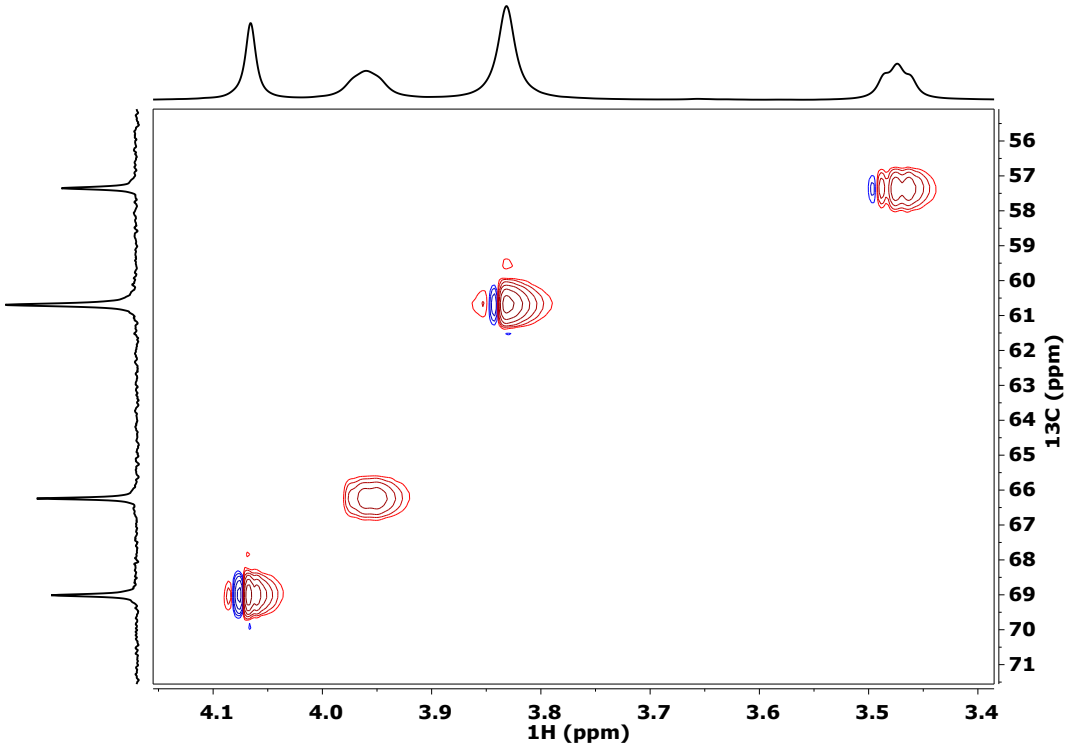

Figure S34. $^{1}H - {}^{13}C$ HSQC spectra of of $[Zn(EGTA)]^{2-}$ complex ([ZnL]=50 mM, pH=7.04, D_2O, 9.4 T, 343 K)

Table S1. NMR spectral parameters for $[Zn(EHDTA)]^{2-}$, $[Zn(OBETA)]^{2-}$ and $[Zn(EGTA)]^{2-}$ complexes (pH=7.0, D_2O)

$[Zn(EHDTA)]^{2-}$	1/1'	2/2'	3	4	5
δ_H / ppm	–	2.82/3.21 2.93/3.01	2.30/2.65	3.92	1.42/1.89
$^2J_{H-H}$ / Hz	–	16.0/ 16.0	11.6/10.8	–	–
δ_C / ppm	177.4/177.9	56.9/61.2	60.7	74.1	28.3
$[Zn(OBETA)]^{2-}$	**1/1'**	**2/2'**	**3**	**4**	
δ_H / ppm	–	2.89/2.95	2.59	3.15	
$^2J_{H-H}$ / Hz	–	16.3	–	–	
δ_C / ppm	178.1	60.1	57.2	64.5	
$[Zn(EGTA)]^{2-}$	**1/1'**	**2/2'**	**3**	**4**	**5**
δ_H / ppm	–	3.80	3.45	3.95	4.05
$^2J_{H-H}$ / Hz	–	–	–	–	–
δ_C / ppm	177.3/179.2	58.9/60.8	56.8	65.2	68.1

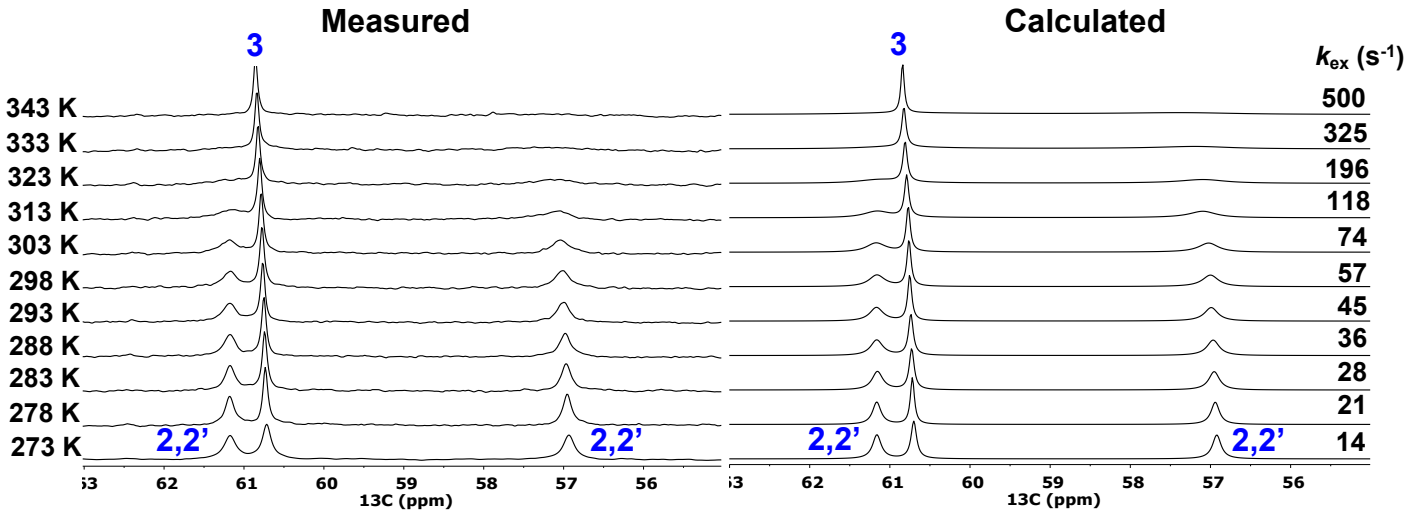

Figure S35. Measured and calculated VT-^{13}C NMR spectra of $[Zn(EHDTA)]^{2-}$ in the temperature range 298 - 343 K ([ZnL]=50 mM, pH=7.10, 9.4 T, D_2O)

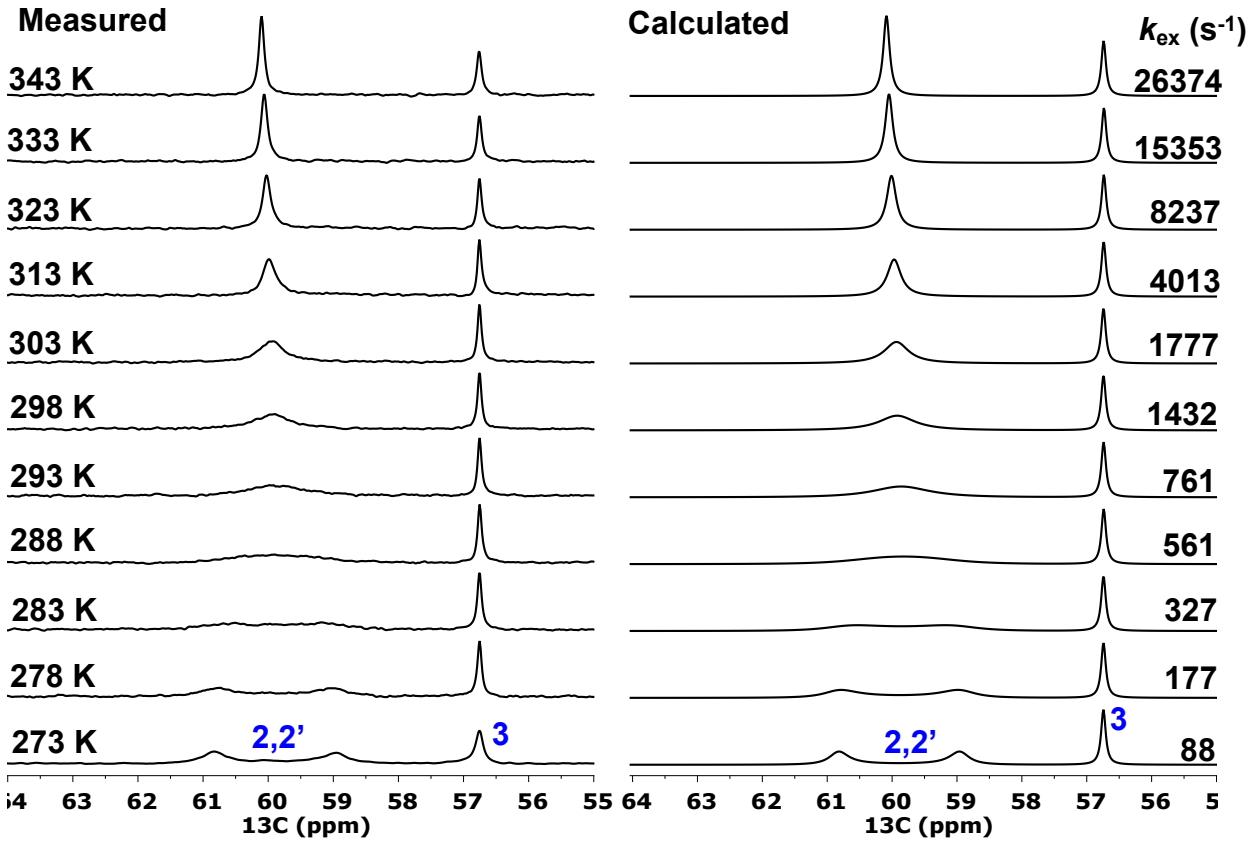

Figure S36. Measured and calculated VT-^{13}C NMR spectra of $[Zn(EGTA)]^{2-}$ in the temperature range 298 - 343 K ([ZnL]=50 mM, pH=7.04, 9.4 T, D_2O)

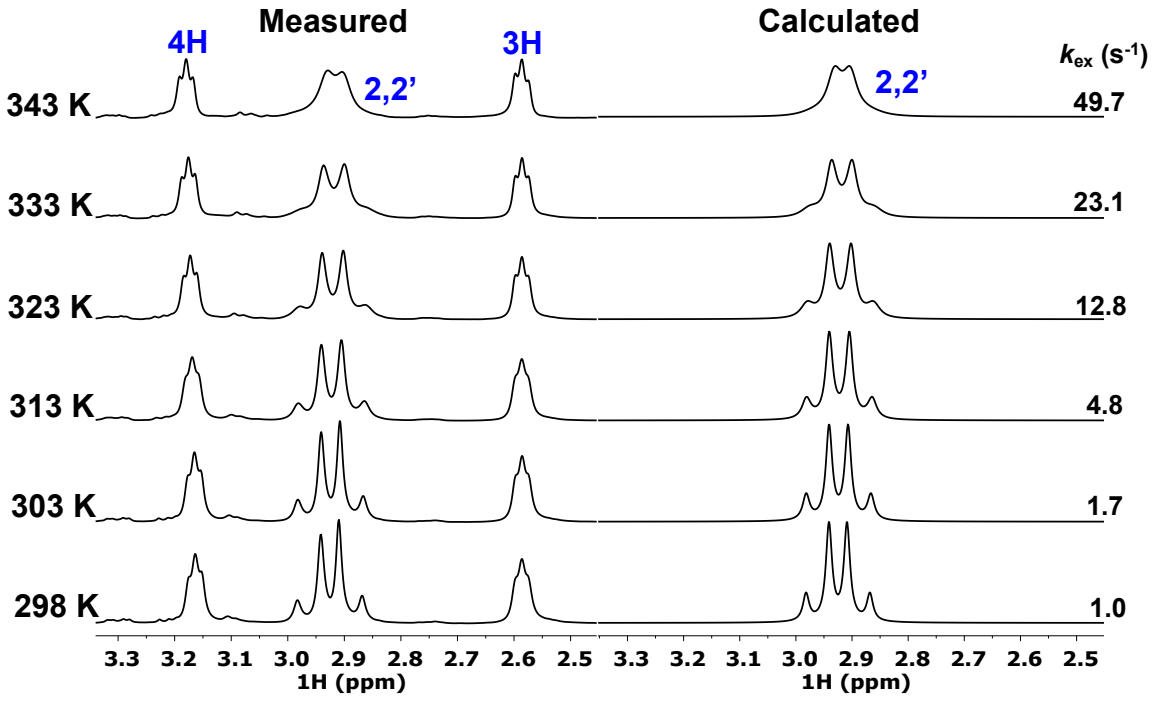

Figure S37. Measured and calculated VT-^{1}H NMR spectra of $[Zn(OBETA)]^{2-}$ in the temperature range 298 - 343 K ([ZnL]=50 mM, pH=7.01, 9.4 T, D_2O)

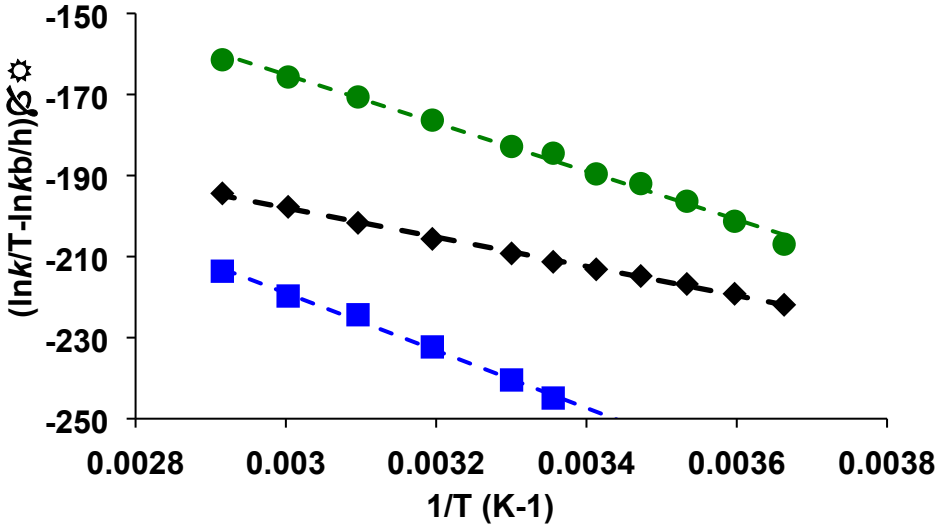

Figure S38. *Eyring* plot for determining the activation parameters of the isomerization processes in **[Zn(EHDTA)]$^{2-}$**, **[Zn(OBETA)]$^{2-}$** and **[Zn(EGTA)]$^{2-}$**

DFT calculations

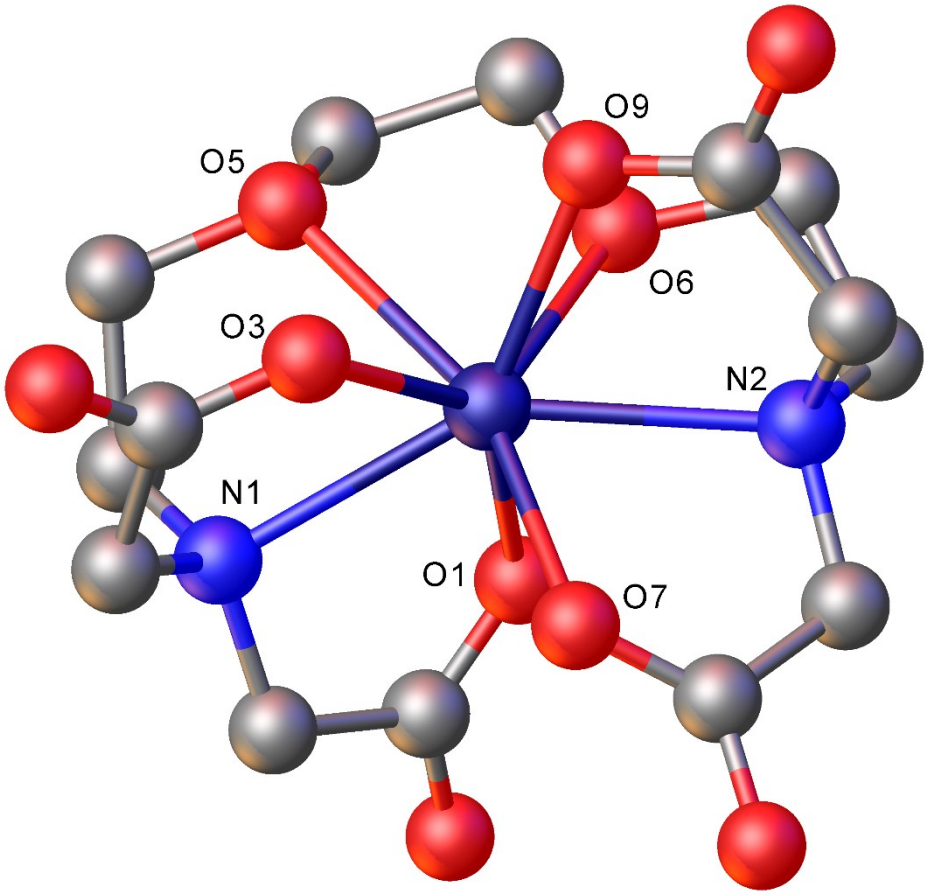

Figure S39. Structure of the $[Mn(EGTA)]^{2-}$ complex observed by X-ray diffraction in $Sr[Mn(EGTA)]\cdot 7H_2O$. Data taken from Ref [5]. Hydrogen atoms were omitted for simplicity.

Table S2. Bond distances (Å) of the metal coordination environment in $[M(EGTA)]^{2-}$ complexes (M = Mn or Zn).

	$[Mn(EGTA)]^{2-}$ (X-ray)	$[Mn(EGTA)]^{2-}$ (DFT)	$[Zn(EGTA)]^{2-}$ (DFT)
M-N1	2.427	2.495	2.527
M-N2	2.426	2.507	2.400
M-O1	2.211	2.196	2.073
M-O3	2.256	2.195	2.086
M-O5	2.495	2.705	3.011
M-O6	2.529	2.542	2.555
M-O7	2.285	2.229	2.183
M-O9	2.233	2.237	2.146

[a] Data from Ref [5].

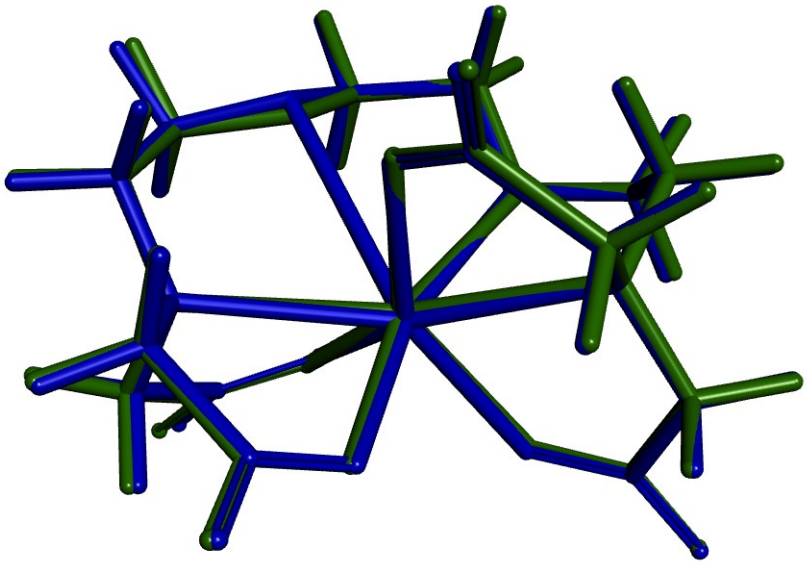

Figure S40. Superimposition of the structures of $[Mn(EGTA)]^{2-}$ (green) and $[Zn(EGTA)]^{2-}$ (blue) obtained with DFT calculations.

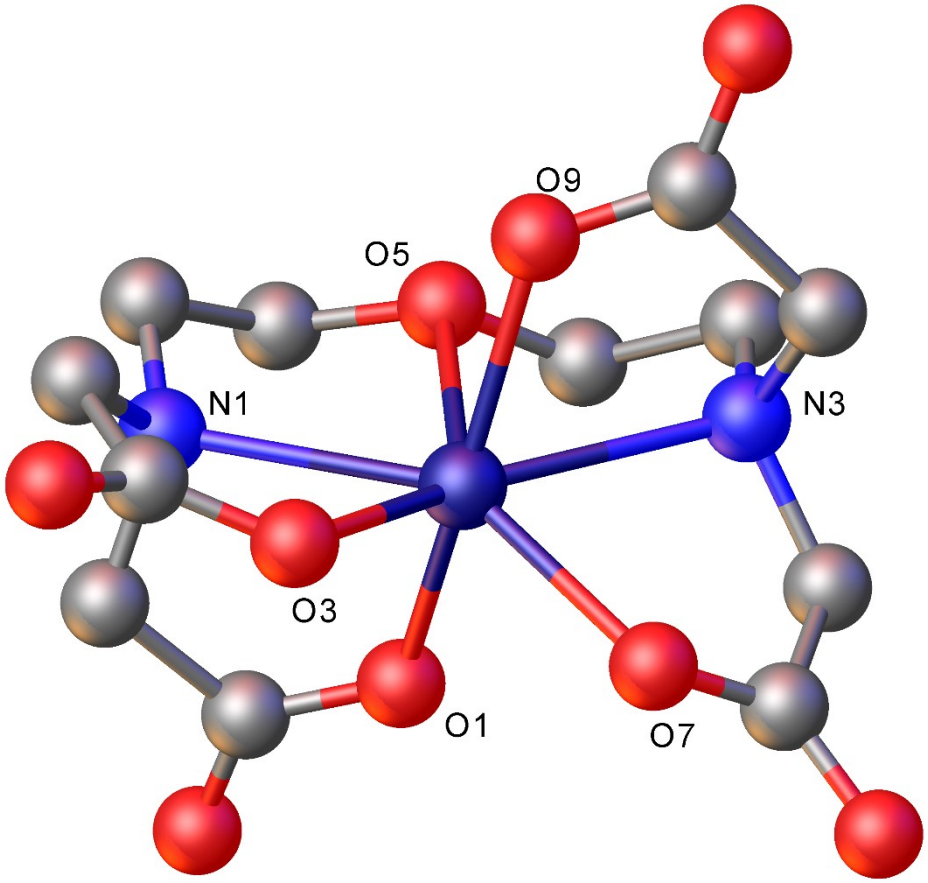

Figure S41. Structure of the $[Mn(OBETA)]^{2-}$ obtained with DFT calculations. Hydrogen atoms omitted for simplicity.

Table S3. Bond distances (Å) of the metal coordination environment in $[M(OBETA)]^{2-}$ and $[M(EHDTA)]^{2-}$ complexes obtained with DFT (M = Mn or Zn).

	$[Mn(OBETA)]^{2-}$	$[Zn(OBETA)]^{2-}$	$[Mn(EHDTA)]^{2-}$	$[Zn(EHDTA)]^{2-}$
M-N1	2.450	2.376	2.519	2.350
M-N2	2.440	2.407	2.395	2.245
M-O1	2.162	2.060	2.210	2.130
M-O3	2.178	2.105	2.166	2.089
M-O5	2.642	2.916	2.417	3.085
M-O7	2.194	2.108	2.198	2.101
M-O9	2.150	2.044	2.193	2.085

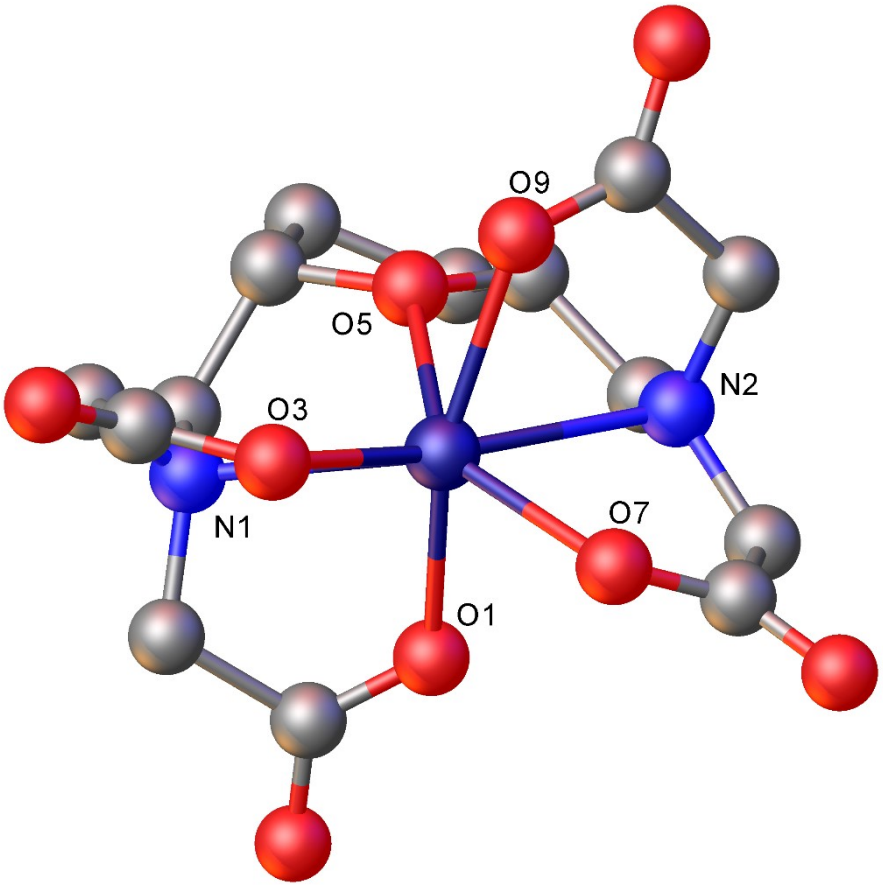

Figure S42. Structure of the $[Mn(EHDTA)]^{2-}$ obtained with DFT calculations. Hydrogen atoms omitted for simplicity.

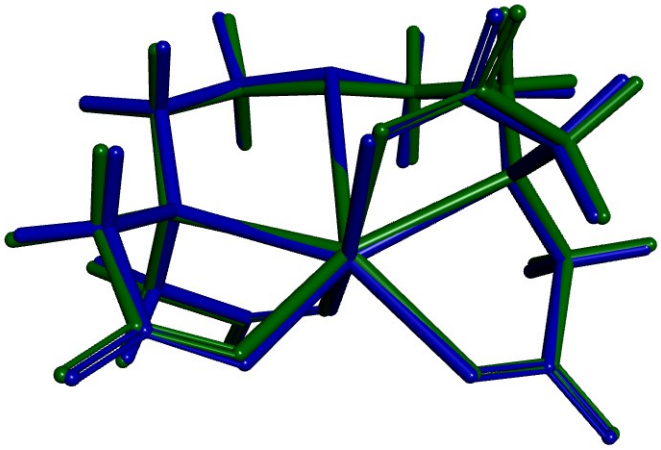

Figure S43. Superimposition of the structures of $[Mn(EGTA)]^{2-}$ (green) and $[Zn(EGTA)]^{2-}$ (blue) obtained with DFT calculations.

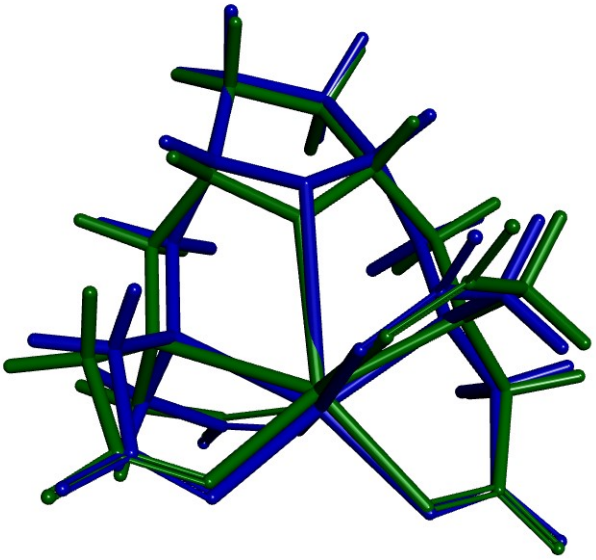

Figure S44. Superimposition of the structures of $[Mn(EHDTA)]^{2-}$ (green) and $[Zn(EHDTA)]^{2-}$ (blue) obtained with DFT calculations.

References

1 J. B. Binder and R. T. Raines, Simple Chemical Transformation of Lignocellulosic Biomass into Furans for Fuels and Chemicals, *J. Am. Chem. Soc.*, 2009, **131**, 1979–1985.

2 W. N. Haworth, W. G. M. Jones and L. F. Wiggins, 1. The conversion of sucrose into furan compounds. Part II. Some 2 : 5-disubstituted tetrahydrofurans and their products of ring scission, *J. Chem. Soc.*, 1945, 1–4.

3 F. K. Kálmán and G. Tircsó, Kinetic Inertness of the Mn^{2+} Complexes Formed with AAZTA and Some Open-Chain EDTA Derivatives, *Inorg. Chem.*, 2012, **51**, 10065–10067.

4 Z. Garda, E. Molnár, F. K. Kálmán, R. Botár, V. Nagy, Z. Baranyai, E. Brücher, Z. Kovács, I. Tóth and G. Tircsó, Effect of the Nature of Donor Atoms on the Thermodynamic, Kinetic and Relaxation Properties of Mn(II) Complexes Formed With Some Trisubstituted 12-Membered Macrocyclic Ligands, *Front. Chem.*, 2018, **6**, 232.

5 C. K. Schauer and O. P. Anderson, Polydentate chelates. 3. Structures of $egta^{4-}$ chelates of manganese(II) and copper(II): $Sr[Mn(egta)]\cdot 7H_2O$ and $[Cu_2(egta)(OH_2)_2]\cdot 2H_2O$, *Acta Crystallogr C Cryst Struct Commun*, 1988, **44**, 981–986.